NASA TECHNICAL NOTE

NASA TN D-4537
C. 1

AN ANALYTICAL INVESTIGATION OF THE AERODYNAMIC AND PERFORMANCE CHARACTERISTICS OF AN UNPOWERED ROTOR ENTRY VEHICLE

by Alan D. Levin and Ronald C. Smith

Ames Research Center
Moffett Field, Calif.

NATIONAL AERONAUTICS AND SPACE ADMINISTRATION • WASHINGTON, D. C. • APRIL 1968

AN ANALYTICAL INVESTIGATION OF THE AERODYNAMIC AND

PERFORMANCE CHARACTERISTICS OF AN UNPOWERED

ROTOR ENTRY VEHICLE

By Alan D. Levin and Ronald C. Smith

Ames Research Center
Moffett Field, Calif.

NATIONAL AERONAUTICS AND SPACE ADMINISTRATION

AN ANALYTICAL INVESTIGATION OF THE AERODYNAMIC AND

PERFORMANCE CHARACTERISTICS OF AN UNPOWERED

ROTOR ENTRY VEHICLE

By Alan D. Levin and Ronald C. Smith

Ames Research Center

SUMMARY

A theoretical analysis has been made of the aerodynamic characteristics of a rotor in autorotative flight. These characteristics have been combined with those of a capsule to study the performance characteristics of a rotor entry vehicle. Performance parameters such as range, deceleration, and heating were determined for a vehicle entering the atmosphere from earth orbit. The effects of rotor to capsule diameter ratio on the entry parameters and the effect of delaying rotor deployment on the range capability were investigated. Substantial gains in lateral range can be obtained by the addition of a rotor to a lifting capsule while maximum deceleration changes very little. The aerodynamic heating on the rotor was found to be severe enough to require possibly delaying deployment of the rotor until after the peak heating region has been passed. Delaying rotor deployment reduced the lateral range capability.

INTRODUCTION

Space vehicles equipped with a rotor for entering the atmosphere from orbit offer several advantages over other entry techniques, some of which are unique to rotary wings alone. The rotor recovery system has the potential of being the only system which in one unit can perform the functions of drag modulation, stabilization, flight path control, and landing with near zero vertical and horizontal speeds on an unprepared landing site.

The rotor derives these advantages from the fact that the energy it stores during autorotation constitutes the means of providing lift. Folded in the trail position during space flight, the rotor would be deployed at the onset of entry into the atmosphere. When the dynamic pressure became large enough, the rotor would be set into rotation. As the centrifugal force increased, the rotor blades would open farther into the air stream, increasing the rotational rate which, in turn, would cause the blades to open still farther. Finally, equilibrium would be reached when the centrifugal moment equals the aerodynamic moment. Thus, the rotor needs only the oncoming air stream to effect deployment of the blades.

Numerous investigators have reported on the rotor recovery technique. Kretz (ref. 1) discussed the application of rotors to atmospheric entry and recovery problems. Hodson (ref. 2) discussed the results of low-speed wind tunnel tests on a 12- and 14-foot-diameter rotor system. Barzda and Schultz (ref. 3) reported on the results of a series of free-flight drop tests and wind-tunnel tests at supersonic speeds of a rotary-wing decelerator. Other aspects of the rotary-wing recovery technique can be found in references 4 to 6, inclusive.

From the literature on the subject of rotary-wing decelerators, it was found that nearly all of the studies considered using the rotor only for the final approach and touchdown maneuver. A few considered deploying the rotor at transonic speeds, even though wind-tunnel tests had been conducted to a Mach number of about 3 (ref. 3). Only Kretz (ref. 1) had considered deploying a lifting rotor at the time of entry into the atmosphere. Since the rotor has to be carried into orbit for use later during the touchdown maneuver, it became clear that the rotor might also prove useful throughout the entire entry trajectory for modulating drag, reducing deceleration through added lift, and providing an increased lateral range capability. An analytical investigation was undertaken to estimate the rotor aerodynamic characteristics and then to use these in combination with an entry vehicle to determine what gains in performance might be achieved over those of a lifting capsule alone for entry from earth orbit.

NOTATION

A_c capsule area, $\pi D_c^2/4$

A_r rotor disk area, πR^2

b number of blades

C_c' maximum value of c_x

C_D drag coefficient, $\dfrac{\text{drag}}{(1/2)\rho V_\infty^2 A_c}$

C_{D_r} rotor drag coefficient, $\dfrac{\text{rotor drag}}{(1/2)\rho V_\infty^2 A_r}$

C_L lift coefficient, $\dfrac{\text{lift}}{(1/2)\rho V_\infty^2 A_c}$

C_{m_X} rolling-moment coefficient, $\dfrac{M_X}{(1/2)\rho V_\infty^2 A_r R}$

C_{m_Y} pitching-moment coefficient, $\dfrac{M_Y}{(1/2)\rho V_\infty^2 A_r R}$

C_N' maximum value of variable portion of c_n

C_{N_0} value of c_n at $\alpha_s = 0^o$

C_Q rotor torque coefficient, $\dfrac{Q}{(1/2)\rho V_\infty^2 A_r R}$

C_X axial-force coefficient, $\dfrac{X}{(1/2)\rho V_\infty^2 A_r}$

C_Y side-force coefficient, $\dfrac{Y}{(1/2)\rho V_\infty^2 A_r}$

C_Z normal-force coefficient, $\dfrac{Z}{(1/2)\rho V_\infty^2 A_r}$

c blade chord

c_n blade section normal force coefficient

c_x blade section chord force coefficient

D diameter

dm blade mass element

e flapping hinge offset

F_P blade local force normal to surface swept by the rotor

F_T blade local force tangent to surface swept by the rotor

h_e entry altitude

I_1 blade moment of inertia about flapping hinge

L/D lift-drag ratio

M_A aerodynamic moment about flapping hinge

M_{CF} centrifugal moment about flapping hinge

M_X rolling moment

M_Y pitching moment

M_∞ free-stream Mach number

m blade mass per unit length

m_o blade mass at the root

3

m_r blade mass at the tip

Q rotor torque

$\dot{q}$ heating rate

R rotor radius

R_e local blade radius of curvature

r blade spanwise station, measured from flapping hinge

T radiation equilibrium temperature

U local velocity

U_P local velocity component at blade normal to surface swept by rotor

U_T local velocity component at blade tangent to surface swept by rotor

$\dot{V}$ deceleration

V_e entry velocity

V_∞ free-stream velocity

W vehicle weight

X axial force

Y side force

Z normal force

α rotor angle of attack

α_s blade section local angle of attack

β flapping angle

γ entry angle relative to the local horizontal, positive up

ε emissivity

η, φ constants used in expression for blade-section chord-force coefficient

θ blade collective pitch angle

ν Stefan-Boltzmann constant

ξ e/R

4

ρ	mass density of air
σ	rotor solidity, $bc/\pi R$
Φ	bank angle
χ	r/R
ψ	azimuth angle of blade, measured from most aft position
Ω	rotor rotational speed

Subscripts

c	capsule
r	rotor
r+c	rotor plus capsule
max	maximum

THEORY

The aerodynamic characteristics of the rotor alone were analyzed for use in combination with the aerodynamic characteristics of a capsule. The analysis was very much like the approach taken in references 7 through 9 which was based upon blade element theory with Newtonian flow concepts used to represent the local blade forces. Small angle approximations were made on the blade collective pitch angle, θ. In the analysis presented herein, no small-angle assumptions were made in regard to the collective pitch angle so that angles up to 90° might be considered. The equations thus obtained were solved numerically on an IBM 7040/7094 computer system.

The rotor-plus-capsule configuration selected for this study is shown in figure 1, and the blade forces and rotor geometry are shown in figure 2. The geometrical relations shown in figure 2 were then used to obtain the aerodynamic characteristics of a rotor alone. The equations obtained are presented herein, without the steps required to go from the integral form to the analytic solution. For the force representation assumed the integration is straightforward. In general, if the blade section forces cannot be expressed in the form assumed herein, solving the integral equations requires stepwise numerical integration.

For the rotor system considered, the local velocities and section angle of attack are obtained from figure 2:

$$U_P = V_\infty(\sin \alpha \cos \beta - \cos \alpha \sin \beta \cos \psi) \tag{1}$$

5

$$U_T = \Omega R \left[(\chi \cos \beta + \xi) + \frac{V_\infty}{\Omega R} \cos \alpha \sin \psi \right] \tag{2}$$

$$\alpha_S = \theta + \tan^{-1} \frac{U_P}{U_T} \tag{3}$$

where it has been assumed that $r\ddot{\beta} = 0$ (synchronizer linkage forces all blades to have the same coning angle, β).

The blade section normal and chord forces are assumed to be of the form:

$$c_n = C_{N_O} + C_N' \sin^2 \alpha_S \tag{4}$$

$$c_x = C_c' (\cos^2 \alpha_S - \varphi \sin^2 \alpha_S - \eta) \tag{5}$$

This form of the forces may be used to represent Newtonian flow forces.

The local blade forces are given by:

$$dF_P = \frac{1}{2} \rho c R U^2 (c_n \cos \theta - c_x \sin \theta) d\chi \tag{6}$$

$$dF_T = \frac{1}{2} \rho c R U^2 (c_n \sin \theta + c_x \cos \theta) d\chi \tag{7}$$

The following useful forms are obtained from equation (3):

$$U^2 \sin^2 \alpha_S = U_P^2 \cos^2 \theta + 2 U_P U_T \sin \theta \cos \theta + U_T^2 \sin^2 \theta \tag{8}$$

$$U^2 \cos^2 \alpha_S = U_T^2 \cos^2 \theta - 2 U_P U_T \sin \theta \cos \theta + U_P^2 \sin^2 \theta \tag{9}$$

where

$$U^2 = U_P^2 + U_T^2 \tag{10}$$

Derivation of Operating Characteristics

Rotor torque is obtained by integrating the elemental aerodynamic torque about the rotor axis.

$$Q = \frac{bR}{2\pi} \int_0^{2\pi} \int_0^{1-\xi} \frac{dF_T}{d\chi} (\chi \cos \beta + \xi) d\chi \, d\psi \tag{11}$$

6

Substituting equations (1), (2), (4), (5), and (10) into equation (11), performing the indicated integration assuming β is constant and dividing by $(1/2)\rho V_\infty^2 \pi R^3$ results in the expression for the rotor torque coefficient.

$$C_Q = \sigma(1 - \xi)\left\{\left[C_N' \sin^3 \theta + C_c' \cos \theta(\cos^2 \theta - \varphi \sin^2 \theta - \eta) + C_{N_O} \sin \theta\right]\right.$$

$$\left[\frac{(1 - \xi)^3}{4} \cos^3 \beta + \xi(1 - \xi)^2 \cos^2 \beta + \frac{3}{2} \xi^2(1 - \xi)\cos \beta + \xi^3\right]\left(\frac{\Omega R}{V_\infty}\right)^2$$

$$+ \left[C_{N_O} \sin \theta + C_c' \cos \theta(\sin^2 \theta - \varphi \cos^2 \theta - \eta) + C_N' \sin \theta \cos^2 \theta\right]$$

$$\left(\sin^2 \alpha \cos^2 \beta + \frac{\cos^2 \alpha \sin^2 \beta}{2}\right)\left(\frac{1 - \xi}{2} \cos \beta + \xi^2\right)$$

$$+ \sin 2\theta \sin \alpha \cos \beta\left(\frac{\Omega R}{V_\infty}\right)[C_N' \sin \theta - C_c' \cos \theta(1 + \varphi)]$$

$$\left[\frac{(1 - \xi)^2}{3} \cos^2 \beta + \xi(1 - \xi)\cos \beta + \xi^2\right] + \frac{\cos^2 \alpha}{2}$$

$$\left[C_{N_O} \sin \theta + C_c' \cos \theta(\cos^2 \theta - \varphi \sin^2 \theta - \eta) + C_N' \sin^3 \theta\right]$$

$$\left.\left(\frac{1 - \xi}{2} \cos \beta + \xi\right)\right\} \tag{12}$$

The blade centrifugal moment is given by:

$$M_{CF} = R^2 \int_O^{1-\xi} (X \cos \beta + \xi)X \sin \beta \Omega^2 \, dm \tag{13}$$

For a blade with a linear mass distribution:

$$m = m_O\left[1 - (1 - \lambda) \frac{X}{1 - \xi}\right] \tag{14}$$

where

$$\lambda = \frac{m_r}{m_O} \tag{15}$$

and

$$dm = mR \, dX \tag{16}$$

7

Substituting equations (14), (15), and (16) into equation (13) gives

$$M_{CF} = I_1 \Omega^2 \sin \beta \left(\frac{1 + 3\lambda}{4} \cos \beta + \frac{1 + 2\lambda}{2} \frac{\xi}{1 - \xi} \right) \tag{17}$$

where

$$I_1 = \frac{m_0 R^3 (1 - \xi)^3}{3} \tag{18}$$

The aerodynamic moment that tends to raise the coning of one blade is given by:

$$M_A = \frac{R}{2\pi} \int_0^{2\pi} \int_0^{1-\xi} \frac{X dF_P}{dX} dX \, d\psi \tag{19}$$

The integrated expression for the aerodynamic moment is

$$M_A = \frac{1}{4} \rho c R^4 \Omega^2 (1 - \xi)^2 \cos \theta \left\{ \left[(C_{N_0} + C_N' \sin^2 \theta) + C_c' \tan \theta (\eta + \varphi \sin^2 \theta - \cos^2 \theta) \right] \right.$$

$$\left[\frac{(1 - \xi)^2}{2} \cos^2 \beta + \frac{4\xi}{3} (1 - \xi) \cos \beta + \xi^2 + \left(\frac{V_\infty}{\Omega R} \right)^2 \frac{\cos^2 \alpha}{2} \right]$$

$$+ \left[(C_{N_0} + C_N' \cos^2 \theta) + C_c' \tan \theta (\eta + \varphi \cos^2 \theta - \sin^2 \theta) \right] \left(\frac{V_\infty}{\Omega R} \right)^2$$

$$\left(\sin^2 \alpha \cos^2 \beta + \frac{\cos^2 \alpha \sin^2 \beta}{2} \right) + \sin 2\theta \sin \alpha \cos \beta \left(\frac{V_\infty}{\Omega R} \right)$$

$$\left. \left[C_N' + C_c' (1 + \varphi) \tan \theta \right] \left[\frac{2}{3} (1 - \xi) \cos \beta + \xi \right] \right\} \tag{20}$$

For equilibrium coning $M_{CF} = M_A$ and for autorotative torque equilibrium $C_Q = 0$; thus there are two equations in the three unknowns, β, θ, and $\Omega R/V_\infty$. We choose θ as the independent variable, and solve the equations for β and $\Omega R/V_\infty$. The results are substituted into the expressions which follow to determine the aerodynamic force coefficients.

8

Derivation of Aerodynamic Performance Characteristics

The rotor axial, side, and normal forces, respectively, are

$$X = \frac{b}{2\pi} \int_0^{2\pi} \int_0^{1-\xi} \left(\frac{dF_T}{d\chi} \sin\psi - \frac{dF_P}{d\chi} \sin\beta \cos\psi \right) d\chi \, d\psi \tag{21}$$

$$Y = -\frac{b}{2\pi} \int_0^{2\pi} \int_0^{1-\xi} \left(\frac{dF_P}{d\chi} \sin\beta \sin\psi + \frac{dF_T}{d\chi} \cos\psi \right) d\chi \, d\psi \tag{22}$$

$$Z = \frac{b}{2\pi} \int_0^{2\pi} \int_0^{1-\xi} \frac{dF_P}{d\chi} \cos\beta \, d\chi \, d\psi \tag{23}$$

Integrating and dividing by $(1/2)\rho V_\infty^2 \pi R^2$ gives the rotor axial, side, and normal force coefficients, respectively,

$$c_X = \sigma \cos\alpha(1-\xi) \left\{ [\sin\theta(c_{N_O} + c_N' \sin^2\theta) + c_c' \cos\theta(\cos^2\theta - \varphi \sin^2\theta \cos^2\beta - \eta)] \left(\frac{\Omega R}{V_\infty}\right) \left(\frac{1-\xi}{2}\cos\beta + \xi\right) \right.$$
$$+ [(c_N' \tan\theta - c_c')\sin\theta \cos^2\theta + (c_N' \cos^3\theta - c_c' \sin^3\theta)\sin^2\varphi - c_c'\varphi \sin\theta \cos^2\theta \cos^2\beta]\sin\alpha \cos\beta$$
$$\left. + (c_{N_O}\cos\theta + c_c'\eta \sin\theta)\sin\alpha \sin^2\beta \cos\beta + (c_N' + c_c' \tan\theta)\left(\frac{\Omega R}{V_\infty}\right)\sin\theta \cos^2\theta \sin^2\beta \right\} \tag{24}$$

$$c_Y = \sigma \cos\alpha \sin\beta \cos\theta(1-\xi) \left\{ \left[c_c' \frac{\sin 2\theta}{2}(1 - \varphi \sec^2\theta) - c_N' \sin^2\theta - c_c'\eta \tan\theta - c_{N_O} \right]\left(\frac{\Omega R}{V_\infty}\right)\left(\frac{1-\xi}{2}\cos\beta + \xi\right) \right.$$
$$\left. + [c_{N_O}\tan\theta - c_c'(\eta + \varphi)]\sin\alpha \cos\beta + (c_N' \sin\theta - c_c' \cos\theta)\left(\frac{\Omega R}{V_\infty}\right)\sin\theta \right\} \tag{25}$$

$$c_Z = \sigma \cos^3\beta \cos\theta(1-\xi) \left\{ [c_{N_O} + c_N' \sin^2\theta + c_c'(\eta \tan\theta - \sin\theta \cos\theta + \varphi \sin^2\theta \tan\theta)] \right.$$
$$\left(\frac{\Omega R}{V_\infty}\right)^2 \left[\frac{(1-\xi)^2}{3} + \xi(1-\xi)\sec\beta + \xi^2 \sec^2\beta \right]$$
$$+ [c_{N_O} + c_N' \cos^2\theta + c_c' \tan\theta(\eta - \sin^2\theta + \varphi \cos^2\theta)]\left(\sin^2\alpha + \cos^2\alpha \frac{\tan^2\beta}{2} \right)$$
$$+ [c_{N_O} + c_N' \sin^2\theta + c_c' \tan\theta(\eta - \cos^2\theta + \varphi \sin^2\theta)]\frac{\cos^2\alpha}{2}\sec^2\beta$$
$$\left. + 2\sin\theta \sin\alpha\left(\frac{\Omega R}{V_\infty}\right)[c_N' \cos\theta + c_c'(1+\varphi)\sin\theta]\left(\frac{1-\xi}{2} + \xi \sec\beta\right) \right\} \tag{26}$$

The rotor rolling and pitching moment about the hub are

$$M_X = -\frac{bR}{2\pi} \int_0^{2\pi} \int_0^{1-\xi} \left[\frac{dF_P}{d\chi}(\chi + \xi \cos\beta)\sin\psi + \frac{dF_T}{d\chi}\chi \sin\beta \cos\psi \right] d\chi \, d\psi \tag{27}$$

$$M_Y = \frac{bR}{2\pi} \int_0^{2\pi} \int_0^{1-\xi} \left[\frac{dF_T}{d\chi}\chi \sin\beta \sin\psi - \frac{dF_P}{d\chi}(\chi + \xi \cos\beta)\cos\psi \right] d\chi \, d\psi \tag{28}$$

Integrating and dividing by $(1/2)\rho V_\infty^2 \pi R^3$ gives the rotor rolling and pitching moment coefficients about the hub

$$
\begin{aligned}
c_{m_X} = -\sigma \cos\alpha \cos\theta \cos\beta(1-\xi)^2 &\left\{ [C_N' + C_C'(1+\varphi)\tan\theta] \frac{\sin 2\theta}{2} \sin\alpha\left(\frac{1}{2} + \frac{\xi}{1-\xi}\cos\beta\right) \right. \\
&+ \left[C_{N_O} + C_N'\sin^2\theta + C_C'\tan\theta(\eta - \cos^2\theta + \varphi\sin^2\theta)\right]\left(\frac{\Omega R}{V_\infty}\right)\left[\frac{1-\xi}{3} + \frac{\xi}{2}\sec\beta(1+\cos^2\beta) + \frac{\xi^2}{1-\xi}\right] \\
&- \left[C_{N_O}\tan\theta - C_C'(\eta + \varphi\cos^2\theta) + (C_N' + C_C'\tan\theta)\frac{\sin 2\theta}{2}\right]\frac{\sin\alpha}{2}\sin^2\beta \\
&\left. - \left[C_N'\tan\theta - C_C'(1+\varphi)\right]\frac{\sin 2\theta}{2}\sin^2\beta\left(\frac{\Omega R}{V_\infty}\right)\left(\frac{1-\xi}{3} + \frac{\xi}{2}\sec\beta\right)\right\}
\end{aligned}
\tag{29}
$$

$$
\begin{aligned}
c_{m_Y} = \sigma \cos\alpha \cos\theta \frac{\sin 2\beta}{2}(1-\xi)^2 &\left\{ [C_N' + C_C'\tan\theta(1+\varphi)]\frac{\sin 2\theta}{2}\left(\frac{\Omega R}{V_\infty}\right)\left[\frac{1-\xi}{3} + \frac{\xi}{2}\sec\beta(1+\cos^2\beta) + \frac{\xi^2}{1-\xi}\right] \right. \\
&+ \left[\tan\theta(C_{N_O} + C_N'\sin^2\theta) + C_C'(\cos^2\theta - \varphi\sin^2\theta - \eta)\right]\left(\frac{\Omega R}{V_\infty}\right)\left(\frac{1-\xi}{3} + \frac{\xi}{2}\sec\beta\right) \\
&+ \left[C_{N_O} + C_N'\cos^2\theta + C_C'\tan\theta(\eta - \sin^2\theta + \varphi\cos^2\theta)\right]\left(\frac{1}{2} + \frac{\xi}{1-\xi}\cos\beta\right)\sin\alpha \\
&\left. + \frac{\sin 2\theta}{4}\sin\alpha[C_N'\tan\theta - C_C'(1+\varphi)]\right\}
\end{aligned}
\tag{30}
$$

The rotor lift-drag ratio is computed from

$$
\frac{L}{D} = \frac{C_Z \cos\alpha - C_X \sin\alpha}{C_X \cos\alpha + C_Z \sin\alpha}
\tag{31}
$$

Theoretical Solution for Axial Flow

For the special case of $\alpha = 90°$ (the nonlifting case), $\lambda = 1$ and $C_{N_O} = \eta = \varphi = \xi = 0$, the equations reduce to a very simplified form. Here no simultaneous solution of equations is required to obtain the equlibrium values for β and $\Omega R/V_\infty$, and the equations become

$$
\begin{aligned}
C_Q = \sigma \cos^3\beta &\left[(C_N'\tan^3\theta + C_C')\left(\frac{\Omega R}{V_\infty}\right)^2 + \frac{8}{3}\left(\frac{\Omega R}{V_\infty}\right)(C_N'\tan^2\theta - C_C'\tan\theta)\right. \\
&\left. + 2(C_N'\tan\theta + C_C'\tan^2\theta)\right] = 0
\end{aligned}
\tag{32}
$$

$$
M_{CF} = \frac{I_1\Omega^2}{2}\sin 2\beta
\tag{33}
$$

$$
\begin{aligned}
M_A = \frac{1}{4}\rho c R^4 \Omega^2 &\left[\frac{1}{2}\tan\theta(C_N'\tan\theta - C_C') + (C_N' - C_C'\tan^3\theta)\left(\frac{V_\infty}{\Omega R}\right)^2 \right. \\
&\left. + \frac{4}{3}\tan\theta(C_N' + C_C'\tan\theta)\left(\frac{V_\infty}{\Omega R}\right)\right]
\end{aligned}
\tag{34}
$$

$$
\begin{aligned}
C_Z = \sigma \cos^3\beta \cos^3\theta &\left[\frac{\tan\theta}{3}(C_N'\tan\theta - C_C')\left(\frac{\Omega R}{V_\infty}\right)^2 + (C_N' - C_C'\tan^3\theta) \right. \\
&\left. + \tan\theta(C_N' + C_C'\tan\theta)\left(\frac{\Omega R}{V_\infty}\right)\right] \equiv C_D
\end{aligned}
\tag{35}
$$

and $C_X = C_Y = C_{m_X} = C_{m_Y} = L/D = 0$.

10

Equation (32) is solved for the equilibrium value of $\Omega R/V_\infty$ as a function of θ, independent of the value of β. Equation (33) is equated to equation (34) and the value of $\Omega R/V_\infty$ obtained from equation (32) is used to find the equilibrium coning angle, β.

Vehicle Performance Characteristics

Aerodynamic characteristics.- The results from the theoretical analysis of aerodynamic characteristics of the rotor alone were combined with the capsule aerodynamic characteristics in order to obtain the combined rotor-plus-capsule characteristics. The capsule area is used as the reference area since it remains constant, whereas the rotor disk area may vary as a result of coning. For the lifting entry the results were combined linearly, as follows:

$$C_{D_{r+c}} = C_{D_c} + C_{D_r} \frac{A_r}{A_c}$$

$$\left(\frac{L}{D}\right)_{r+c} = \frac{C_{L_c} + C_{L_r}(A_r/A_c)}{C_{D_{r+c}}}$$

For the nonlifting entry, since the vehicle was alined with the flight path, a first-order interference correction to account for the area shielded by the capsule was made to the combined drag coefficient of the rotor plus capsule as follows:

$$C_{D_{r+c}} = C_{D_c} + C_{D_r}\left(\frac{A_r}{A_c} - 1\right)$$

Atmospheric entry performance.- A machine program was used to obtain the entry trajectory characteristics. This three-dimensional program included the effects of earth oblateness and rotation and it was assumed that the earth's atmosphere rotated with the earth. The aerodynamic characteristics obtained from the above relations were programmed as tabulated functions of the relative velocity (i.e., of the velocity relative to the rotating atmosphere).

RESULTS AND DISCUSSION

To analyze the performance characteristics of a rotor entry vehicle it was first necessary to obtain the rotor operating characteristics. Once these characteristics had been determined the present theory was used to obtain the rotor aerodynamic characteristics for the conditions of autorotative equilibrium. These aerodynamic characteristics were used to determine the vehicle entry performance characteristics.

Rotor Operating Characteristics

Typical variations of equilibrium dimensionless tip speed with blade pitch are shown in figure 3. Figure 3(a) shows a low-speed operating characteristic which is typical of known data. Note that for the blade pitch range -6° to +9° the tip speed is multivalued, hence an unstable operating range exists. Figure 3(b) shows tip speed data obtained from the present theory for supersonic flight. Data for two values of the ratio C_N'/C_C' are shown for axial flight (α = 90°) and one value for α = 20°. The ratio C_N'/C_C' is a measure of the ratio of elemental driving force to retarding force. This ratio for an airfoil in Newtonian flow equals the chord-to-thickness ratio. Axial flight produced the highest rotor speeds and the greatest sensitivity to pitch change near zero pitch. Accordingly, very accurate pitch control will be needed in this range during axial flight in order to avoid accidental overspeeding. These predicted rotor speeds are single valued and hence stable for any blade pitch angle, something that was not apparent from low-speed rotor characteristics.

Rotor Aerodynamic Characteristics

Figure 4 shows a comparison of theoretical and experimental rotor drag coefficients for the configuration of reference 3 as a function of Mach number for a rotor in axial flight at a tip speed of 107 m/sec (350 ft/sec). Except in the transonic range theory and experiment agree very well. Considering that the theoretical values were based upon Newtonian flow theory, the agreement with the values obtained experimentally is very good at even subsonic Mach numbers.

Vehicle Entry Performance Characteristics

The aerodynamic performance characteristics from the present theory are shown in figure 5. These characteristics were used in the trajectory program to obtain entry performance parameters, such as maximum deceleration, range, and heating rates. The significant results are presented in figures 6 through 8. The capsule-alone configuration was also investigated to provide a basis for comparison. The hypothetical full-scale capsule has a maximum diameter of 3.96 m (13 ft) and weighs 4,535 kg (9,400 lb). The rotor system selected has four blades, a solidity of 0.2, and a diameter of 7.82 m (26 ft). The initial entry conditions used for this study were V_e = 7,610 m/sec (25,000 ft/sec) and h_e = 121,920 m (400,000 ft). Initial entry angles were varied from 0° to -3°.

Range.- Range footprints for the lifting capsule and lifting rotor plus capsule are shown in figure 6 for an entry angle of -3°. Also indicated on the figure is the maximum lateral range for L/D = 1.2, which is obtainable with lifting bodies such as the Ames M-2. The reference for all ranges indicated is the impact point for the nonlifting capsule. The available landing area for the rotor-plus-capsule configuration is about eight times larger than for the lifting capsule alone. The maximum lateral range is

extended from about 170 to nearly 420 n. mi. by the addition of the rotor. The maximum lateral range was obtained by rolling the vehicle to a bank angle of 45° and maintaining this attitude until the heading changed 90° from the entry heading. At that time the vehicle was rolled back to a 0° bank angle and the glide continued to touchdown. Adding the rotor increased the longitudinal range of the capsule from about 1200 to over 1900 n. mi. However, this increase is not so significant as the lateral range increase, since to a large extent longitudinal range can be controlled by controlling the time of retrofire.

Deceleration.- Figure 7 shows the maximum deceleration for the lifting and nonlifting entries as a function of entry angle. They are presented only to show the trends which result from adding a rotor to a capsule. As would be expected, the maximum decelerations encountered increased with steepening of the entry angle. For the nonlifting entry the addition of the rotor reduced the maximum deceleration only about 0.5 g for all entry angles investigated. For the lifting entry, adding a rotor to the capsule did not significantly change the maximum deceleration. Note that the addition of the rotor changes the W/C_DA_c from that for the capsule alone. Hence, the curves shown on figure 7 do not represent a constant value of W/C_DA_c.

Heating.- The rotor blade maximum convective heating rate is presented in figure 8 as a function of entry angle for lifting and nonlifting trajectories of the rotor-plus-capsule and capsule alone. The curves for the capsule-alone trajectories represent deployment of a fictitious rotor at the point of maximum heating on the capsule-alone trajectory and have been included to show the alleviating effect of the rotor on heating. Magnification effects due to the capsule bow shock are not included. The heating rates presented are for a local blade radius of curvature of 0.152 m (6 in.) for the lifting entry and 1.524 m (5 ft) for the nonlifting entry. Radiative heating rates were not computed, but they have been shown to contribute a negligible amount to the overall heating for entry at low earth orbital speeds. A line on the figure indicates the maximum heating rate limit, 463 kW/m^2 (41 Btu/ft^2/sec). This limit is based on radiation equilibrium temperature of 2320° K (3700° F) and has been adjusted by a factor of 2.85 to account for the increase in blade heating behind the capsule bow shock wave. This temperature limit is for a RENE-41 blade structure with a stabilized zirconium oxide coating. This coating is assumed to be satisfactory for operation in this temperature range. It has also been assumed that the coating is sufficient to maintain the RENE-41 structure below its limit of about 1087° K (1500° F). It can be seen from the figure that even for entry at 0° the blade heating rate is too severe. It is also evident from the figure for the nonlifting entry that adding the rotor reduces the maximum heating rate about 20 percent for all entry angles investigated.

Because of the severe nature of the heating of the rotor blades, an investigation was undertaken to determine if increasing the rotor-to-capsule diameter ratio would appreciably reduce the heating. An increase in D_r/D_c reduces W/C_DA_c and should reduce the heating rates even further. The significant results of the effect of diameter ratio on the entry parameters is discussed in the next section.

Effects of diameter ratio on range, deceleration, and heating.- The maximum lateral range as a function of diameter ratio for various entry angles is shown in figure 9. A diameter ratio of 1 represents the capsule alone. There is a very significant effect of diameter ratio up to about $D_r/D_c = 4$. Above $D_r/D_c = 4$, the gain is not nearly so significant and from a weight standpoint further increases in rotor diameter probably would not be worth the small gain in lateral range. This gain can be attributed to increased lift due to the increase in rotor size. For the range of entry angles investigated the maximum lateral range was insensitive to entry angle, the maximum difference being only about 22 n. mi.

It should be noted that autorotative landing studies show that the maximum disk loading tolerable for a reasonable subsonic sink rate, hence a reasonably safe landing, also requires a D_r/D_c in the neighborhood of 3 or more. Increasing $D_r/D_c = 2$ to 4 results in about 140 n. mi. of additional range, an increase of about 33 percent. Whether the increase in range is worth the increased weight and more difficult stowage problem of the larger rotor will depend to a large extent on specific mission requirements. However, it is felt that rotors in the $D_r/D_c = 6 - 10$ size range would not be suitable for any mission because of their size and limited range advantage over a $D_r/D_c = 4$ rotor system.

Figure 10 shows the maximum longitudinal range as a function of diameter ratio for the four entry angles investigated. These ranges are measured from the capsule-alone ballistic impact point, which varied with entry angle. The maximum longitudinal range is more sensitive to entry angle than was the lateral range, as would be expected. From the figure it can be seen that the effect of diameter ratio on the maximum longitudinal range is generally the same as it is for the maximum lateral range. For diameter ratios larger than about 4, the increase in range with further increase in diameter ratio is very small.

The maximum deceleration encountered during entry is presented in figure 11. For nonlifting entry there is a minimum in the maximum deceleration encounted at a diameter ratio of about 4. This minimum is a result of the effect of $W/C_D A_c$. For the lifting entry the maximum deceleration is greatly reduced from the values for the nonlifting entry and is essentially unaffected by diameter ratio for a given entry angle.

The rotor blade maximum convective heating rates for the nonlifting and lifting entries are shown in figures 12(a) and 12(b), respectively. Again the heating rates shown are based on a local radius of curvature of 1.524 m (5 ft) for the nonlifting entry and 0.152 m (6 in.) for the lifting entry. Also shown on figure 12(b) is the rotor blade heating rate limit line which would result in an equilibrium temperature of 2320° K (3700° F). It can be seen that the effect of increasing the diameter ratio is to reduce markedly the heating rate for both the nonlifting and lifting entries. A vehicle with a diameter ratio of 4 has about half the maximum blade heating rate it would have if it were entering on the capsule-alone trajectory ($D_r/D_c = 1$).

Temperatures were obtained from the heating rate data of figures 12(a) and 12(b) by substitution into the relation

14

$$T = \left(\frac{K_1 \dot{q}}{\epsilon \nu}\right)^{1/4}$$

These results are presented in figures 13(a) and 13(b) for the nonlifting and lifting entries, respectively. For computing the temperatures, a value of $\epsilon = 0.8$ was used. The parameter K_1 is a heating-rate multiplication factor which takes into account the blade curvature and the increase in heating rate caused by the capsule's bow shock wave. A value of $K_1 = 2.85$ was obtained analytically, and later experimental results (ref. 10) indicate that this estimate is slightly optimistic. The results of reference 10 indicate a value of about 3.3, except at shock impingement. This 15 percent increase in K_1 would increase the temperatures shown by about 4 percent. For the non-lifting entry a diameter ratio of nearly 4 is required for the temperature limit used. For the lifting entry the diameter ratio required would generally have to be larger than 10.

The indication that the lifting entry would produce excessive temperatures led to the notion of delaying the lifting phase until sometime after peak heating. An additional study was made, therefore, to determine the effect of delayed deployment on range performance.

Effects of delayed deployment.- The effect of delayed deployment on lateral range was investigated for configurations having D_r/D_c of 2 and 4. These results are shown in figures 14 and 15, respectively.

Both lifting and nonlifting modes of capsule operation prior to rotor deployment were investigated and the assumption was made that the vehicle could be banked in the lifting mode prior to rotor deployment. Not being able to utilize the capsule lift resulted in the loss of a substantial portion of the lateral range capability.

The percentage reduction in lateral range resulting from delayed deployment is greater for the $D_r/D_c = 4$ vehicle than for the $D_r/D_c = 2$ vehicle because the diameter ratio 4 vehicle has a higher L/D, which cannot be utilized until the rotor is deployed. For both diameter ratios, the L/D prior to deployment was the same; hence the $D_r/D_c = 4$ vehicle loses a larger percentage of its lateral range capability than does the $D_r/D_c = 2$ vehicle. Shown in figure 16 is the longitudinal range as a function of deployment Mach number for $D_r/D_c = 2$. Curves are shown for both modes of capsule operation prior to deployment. Without being able to utilize capsule lift prior to rotor deployment, the reduction in longitudinal range is considerable even for rotor deployment at a Mach number of 18.

Deploying the rotor at various Mach numbers along the trajectory implies deployment at various heating rate levels. If deployment is made at Mach numbers exceeding about 17 for $D_r/D_c = 4$, the blades would possibly require an ablative coating for heat protection. This is thought to be impractical because of the high probability of nonuniform ablation causing an intolerable vibration level. At deployment Mach numbers above 8, and less than 17, a

coated blade structure similar to the type discussed earlier is required. At deployment Mach numbers below 8, no heat protection is needed.

Figure 17 shows the radiation equilibrium rotor blade temperature as a function of Mach number for a rotor entry vehicle of diameter ratio 4 entering at γ = -2°. With a stabilized zirconium oxide coating having a temperature limit of 2320° K (3700° F), operation of the rotor in the lifting mode must be delayed until a Mach number near 17 is reached.

The results of the investigation led to the development of the sequence of operating modes for the rotor entry vehicle shown in figure 18. At entry the rotor is deployed and the vehicle flown in a near axial attitude with the rotor coned back 45° to avoid capsule bow shock impingement. The heat-transfer results of reference 10 indicate that a coning angle of 45° is required in near axial flight in order to avoid this bow shock impingement. Within this constraint an L/D of nearly 0.3 is possible. At a Mach number of about 16, transition begins to the glide flight (autogyro) attitude and should be completed by the time a Mach number of 14 is reached. From this point to subsonic velocities, supersonic glide flight is maintained at an L/D near 1.0. The subsonic flight portion will be in the L/D = 4.0 range. The vehicle then lands like a helicopter with power off. This sequence of operating modes has not taken into account any potential problems of vehicle trim at the flight attitudes indicated.

CONCLUSIONS

The results of the theoretical investigation of the rotor aerodynamic characteristics and performance of a rotor entry vehicle have led to the following conclusions:

1. The rotor has a stable operating range at low negative blade pitch angles, which was not apparent from low speed helicopter operation.

2. In axial flight the rate of increase of RPM with small blade pitch angle changes is quite severe and will require precise control of blade pitch to prevent overspeeding.

3. In axial flight attitudes there is good agreement between theoretical and experimental rotor drag at least for subsonic and supersonic speeds.

4. When used throughout the entire entry trajectory in a glide mode, the rotor added to the capsule results in substantial gains in lateral range.

5. On the basis of gains in maximum range and magnitude of the maximum decelerations, the most optimum rotor-to-capsule diameter ratio is about 4.

6. From a heating standpoint, the vehicle cannot be used in the glide mode throughout the entire entry trajectory and maintain the temperature constraint of 2320° K (3700° F) on the rotor blade coating.

16

7. Since bow shock impingement on the rotor blades can cause heating rates eight times that of the capsule stagnation value, the rotor may have to be coned back during the peak heating portion of the entry trajectory, thus reducing available rotor thrust.

8. Delaying rotor deployment causes large reductions in the maximum lateral range capability. However, if capsule lift can be utilized prior to rotor deployment, the loss in lateral range is reduced.

Ames Research Center
    National Aeronautics and Space Administration
        Moffett Field, Calif., 94035, Jan. 18, 1968
            124-07-03-04-00-21

REFERENCES

1. Kretz, M.: Application of Rotary Wing Techniques to Atmospheric Re-entry and Launch Vehicle Recovery Problems. Paper presented at European Symposium on Space Technology, London, England, June 1961.

2. Hodson, James S.: Low Speed Wind Tunnel Test of 12-foot and 14-foot Diameter Rotochutes. Kaman Aircraft Corp. Report T-93, Jan. 1957.

3. Barzda, J. J.; and Schultz, E. R.: Test Results of Rotary-Wing Decelerator Feasibility Studies for Capsule Recovery Applications. SAE Paper No. 756D, September 1963.

4. Haig, Chester R., Jr.: The Use of Rotors for the Landing and Reentry Braking of Manned Spacecraft. IAS Paper 60-17, 1960.

5. Galigher, L. L.: Wind Tunnel Tests of the Kaman KRC-6M Rotochute at Supersonic Speeds. AEDC-TDR-63-128, July 1963.

6. Robinson, D. W., et al.: Investigation of Stored Energy Rotors for Recovery. ASD-TDR-63-745, Dec. 1963.

7. Ham, Norman D.: An Experimental and Theoretical Investigation of a Supersonic Rotating Decelerator. J. Am. Helicopter Soc., January 1963, pp. 8-18.

8. Haig, C. R., Jr.: Aerodynamic Analysis of a Rotor in a Fully Stalled Propeller Braking State. Bell Helicopter Report 8008-099-003, March 1960.

9. Haig, C. R., Jr.: An Aerodynamic Analysis of a Lifting Rotor in Hypersonic Flight. Bell Helicopter Report 8008-099-001, June 1959.

10. Smith, Ronald C.; and Levin, Alan D.: Heat-Transfer Measurements on the Rotor Blade of a Rotor Entry Vehicle Model. NASA TN D-4065, 1967.
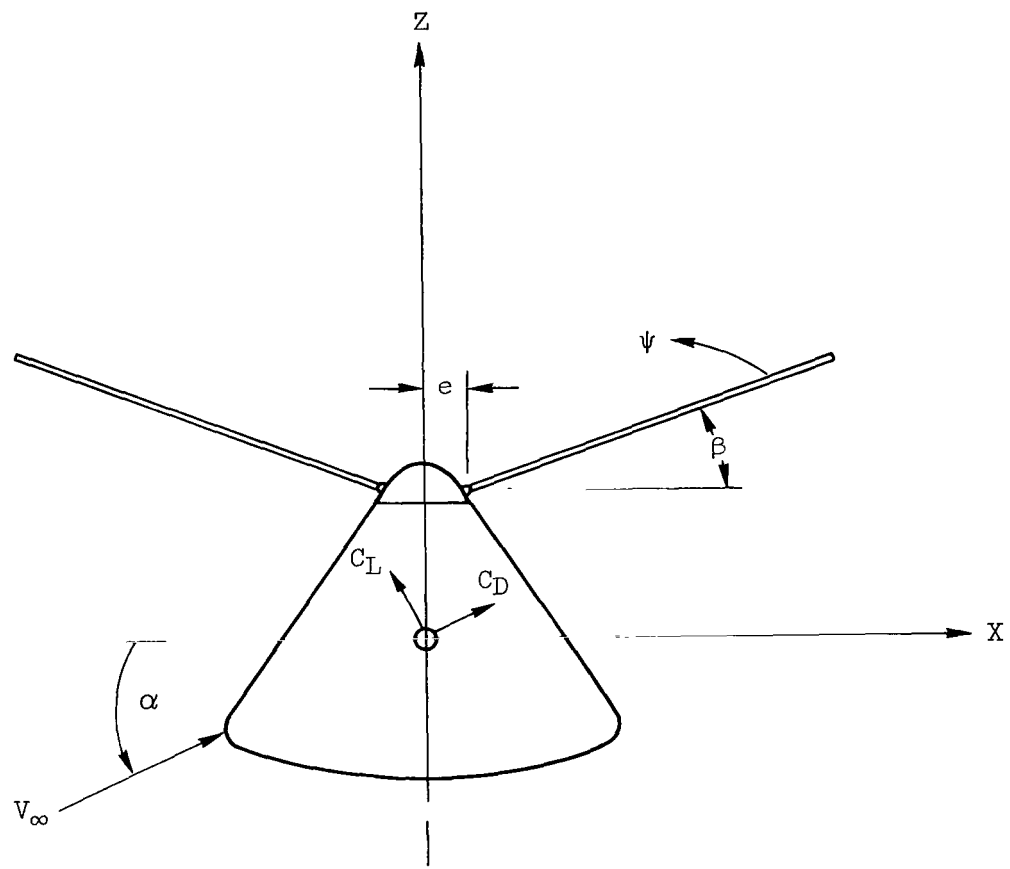
Figure 1.- Study vehicle configuration.
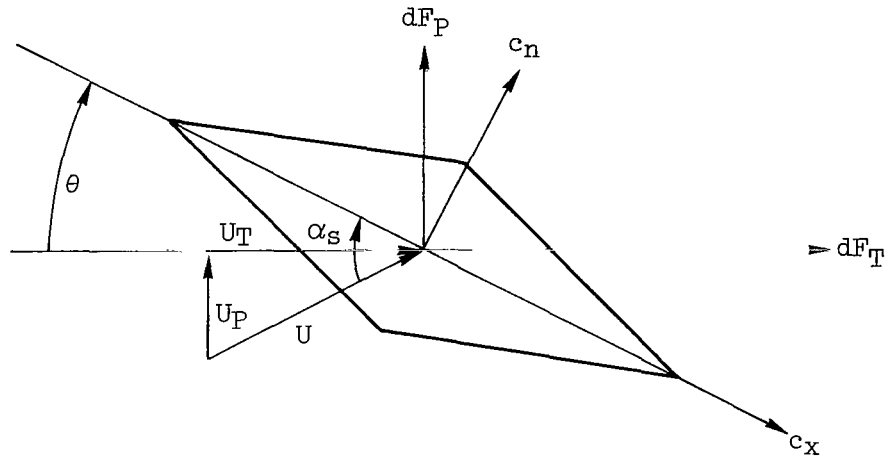
(a) Blade section forces

Figure 2.- Force geometry.
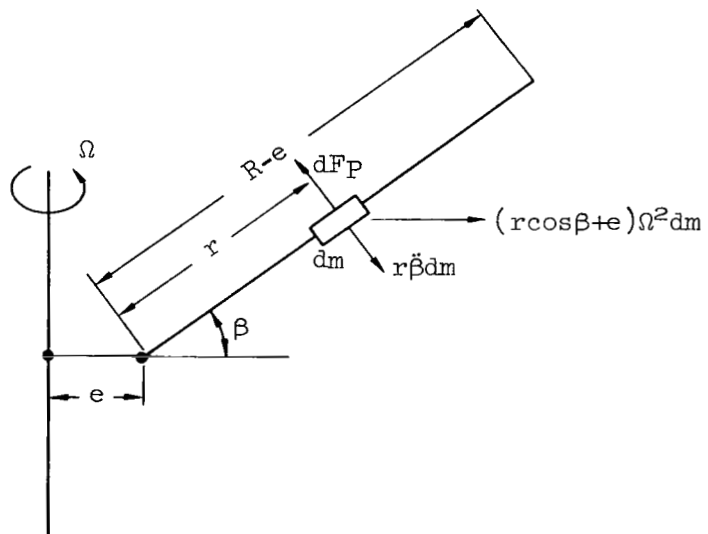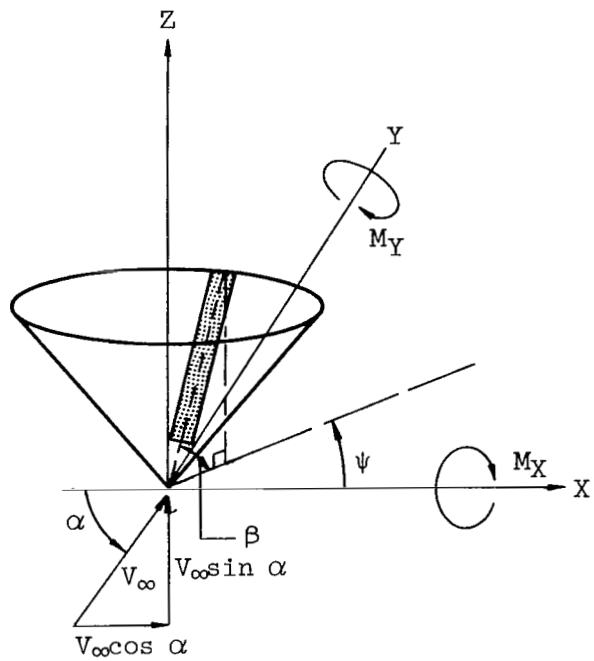
(b) Rotor geometry

Figure 2.- Concluded.

(a) Typical low speed operating
   characteristics

(b) Operating characteristics from
   present theory using "Newtonian"
   section characteristics
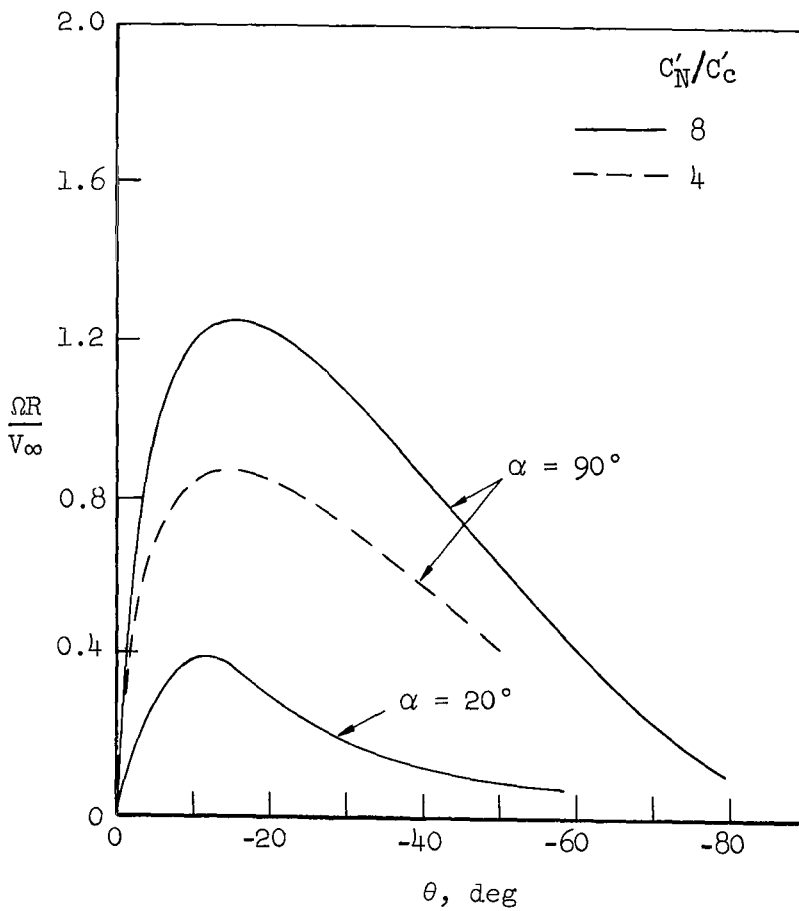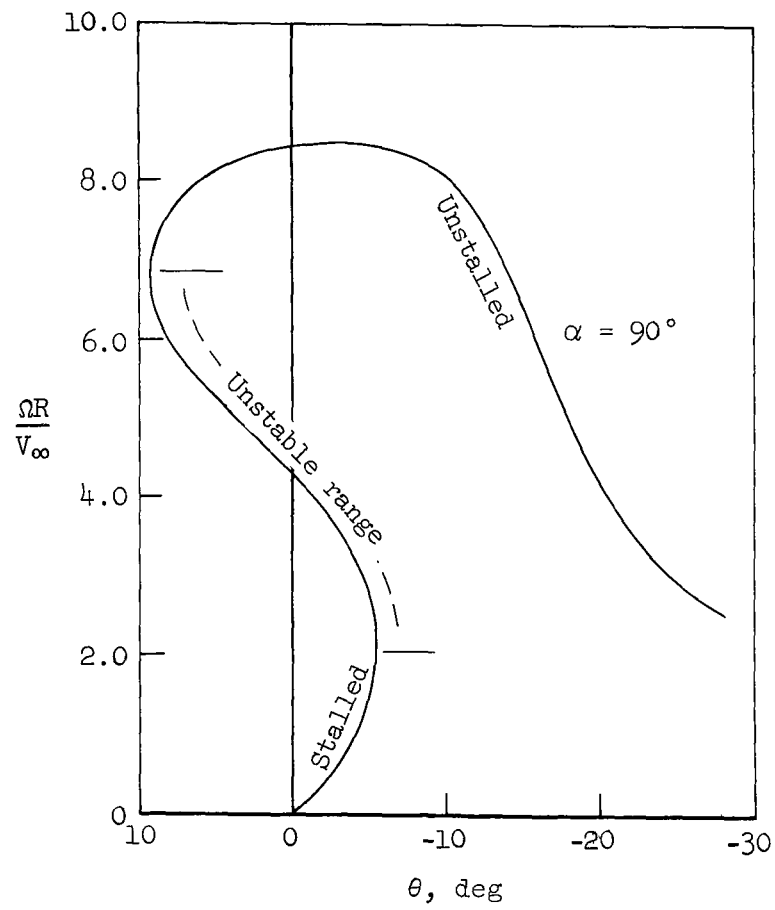
Figure 3.- Variation of autorotative tip speed ratio with blade pitch angle.
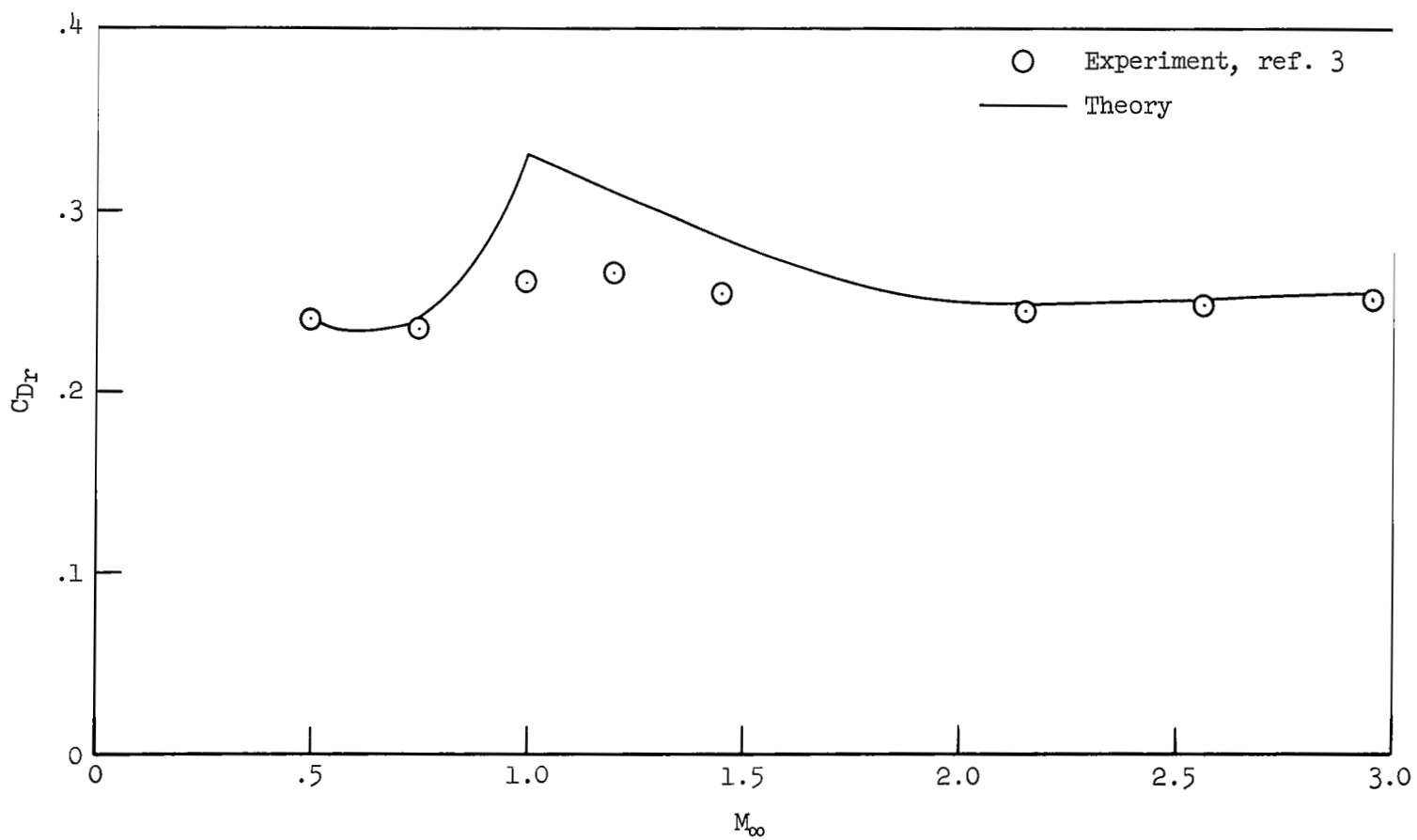
Figure 4.- Comparison of theoretical and experimental rotor drag coefficient; $\alpha = 90°$, $\Omega R = 107$ m/sec (350 ft/sec).
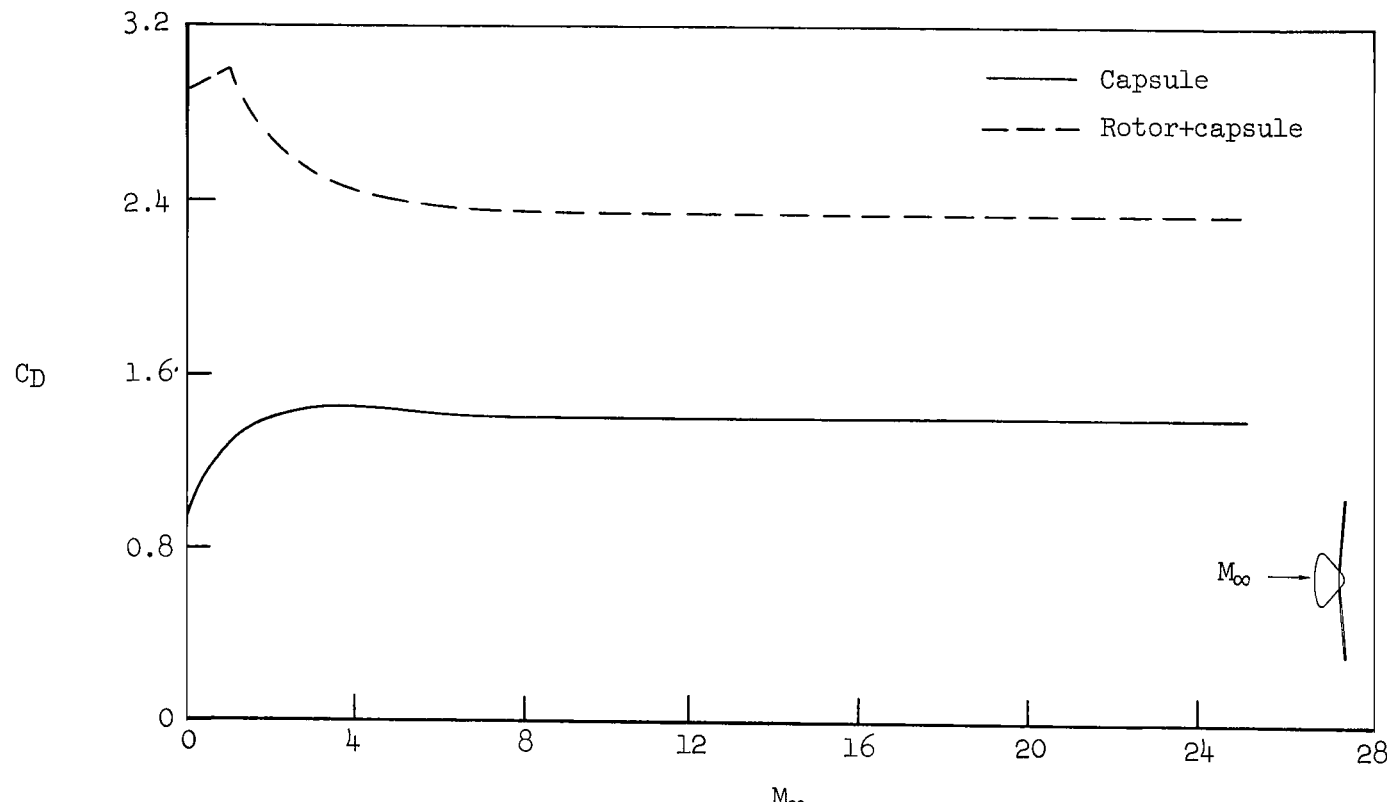
(a) Non lifting

Figure 5.- Aerodynamic characteristics of the study vehicle; $D_r/D_c = 2$.
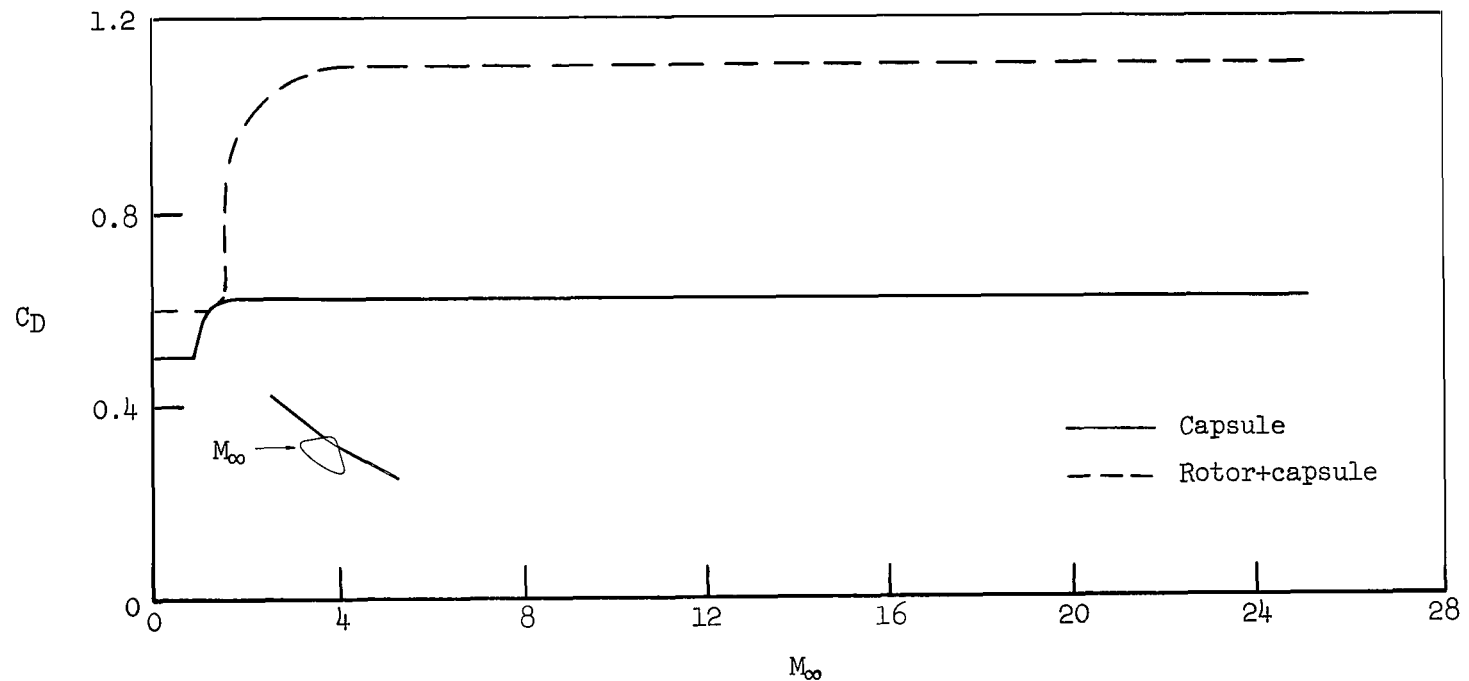
(b) Lifting

Figure 5.- Continued.

(c) Lifting
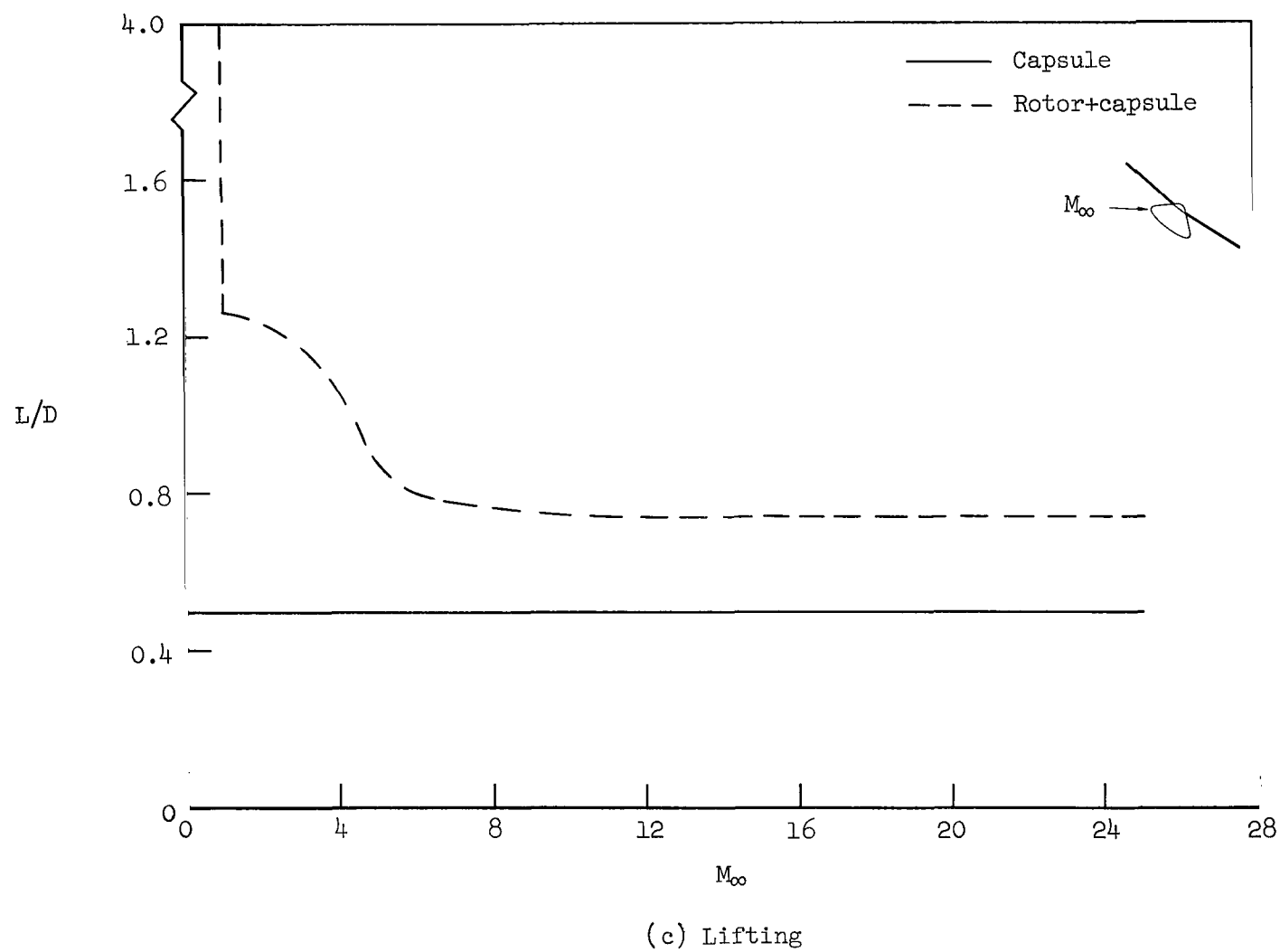
Figure 5.- Concluded.
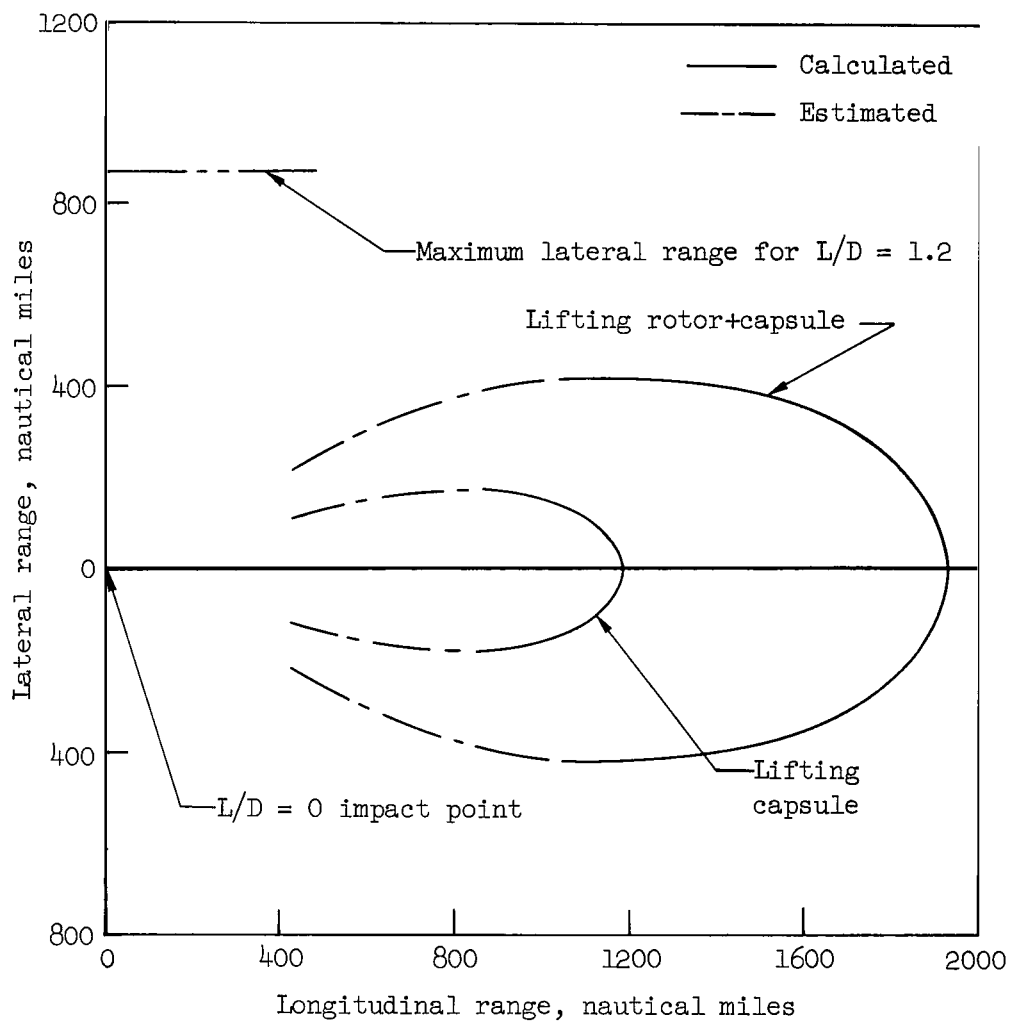
Figure 6.- Typical entry footprints; $\gamma = -3°$, $D_r/D_c = 2$.
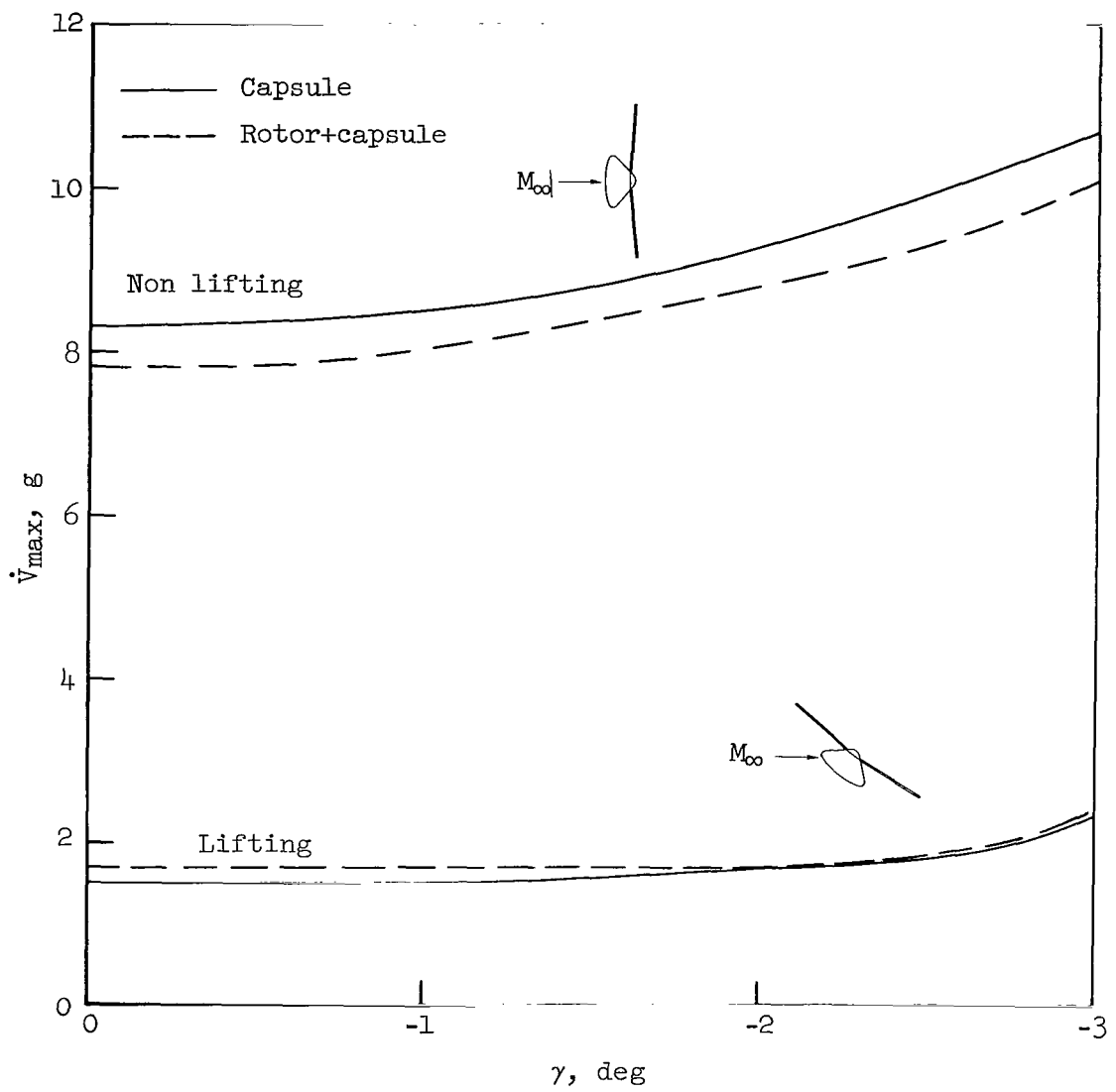
Figure 7.- Maximum deceleration; $D_r/D_c = 2$.
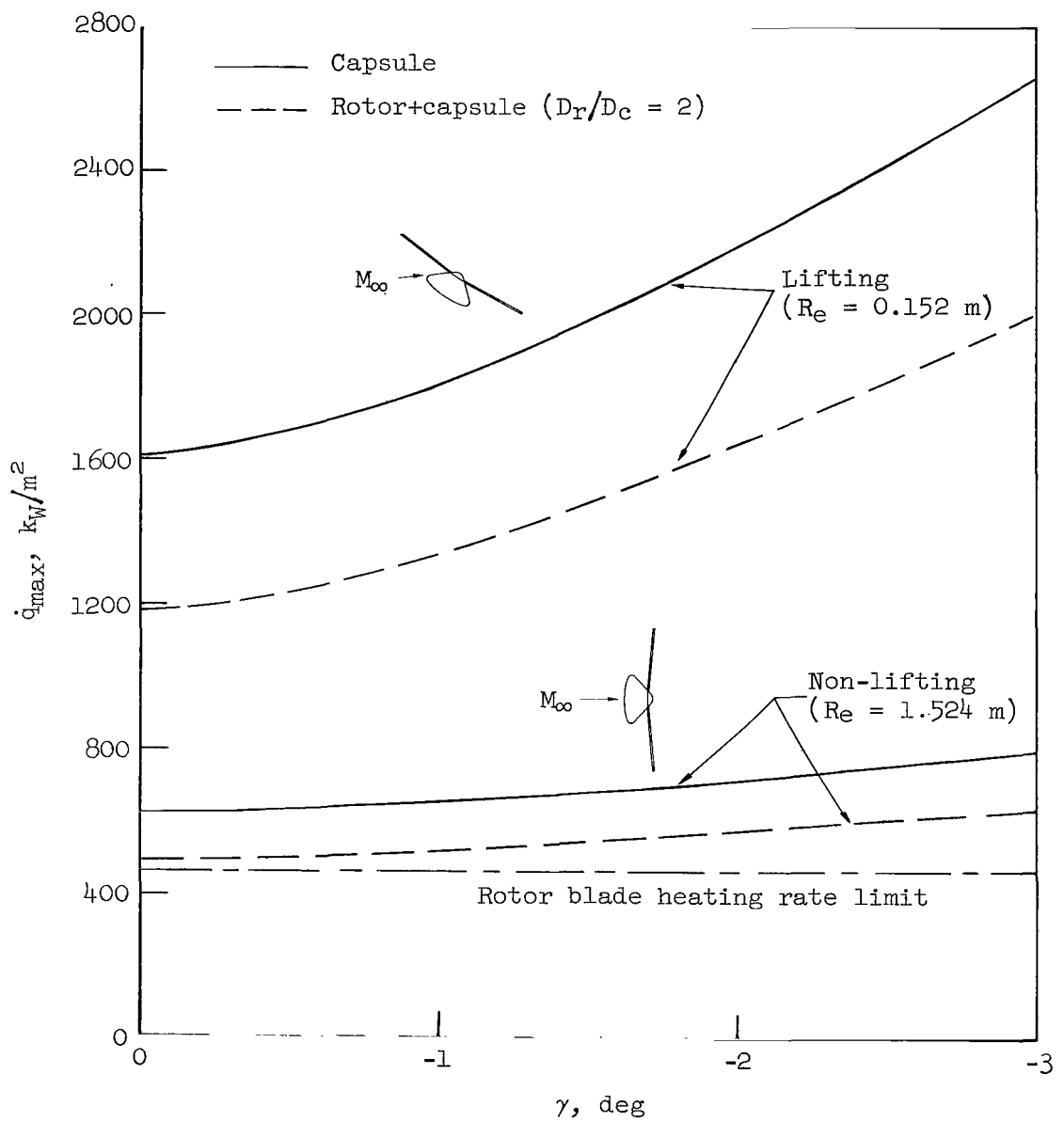
Figure 8.- Rotor blade maximum convective heating rate for rotor-plus-capsule and capsule-alone trajectories.
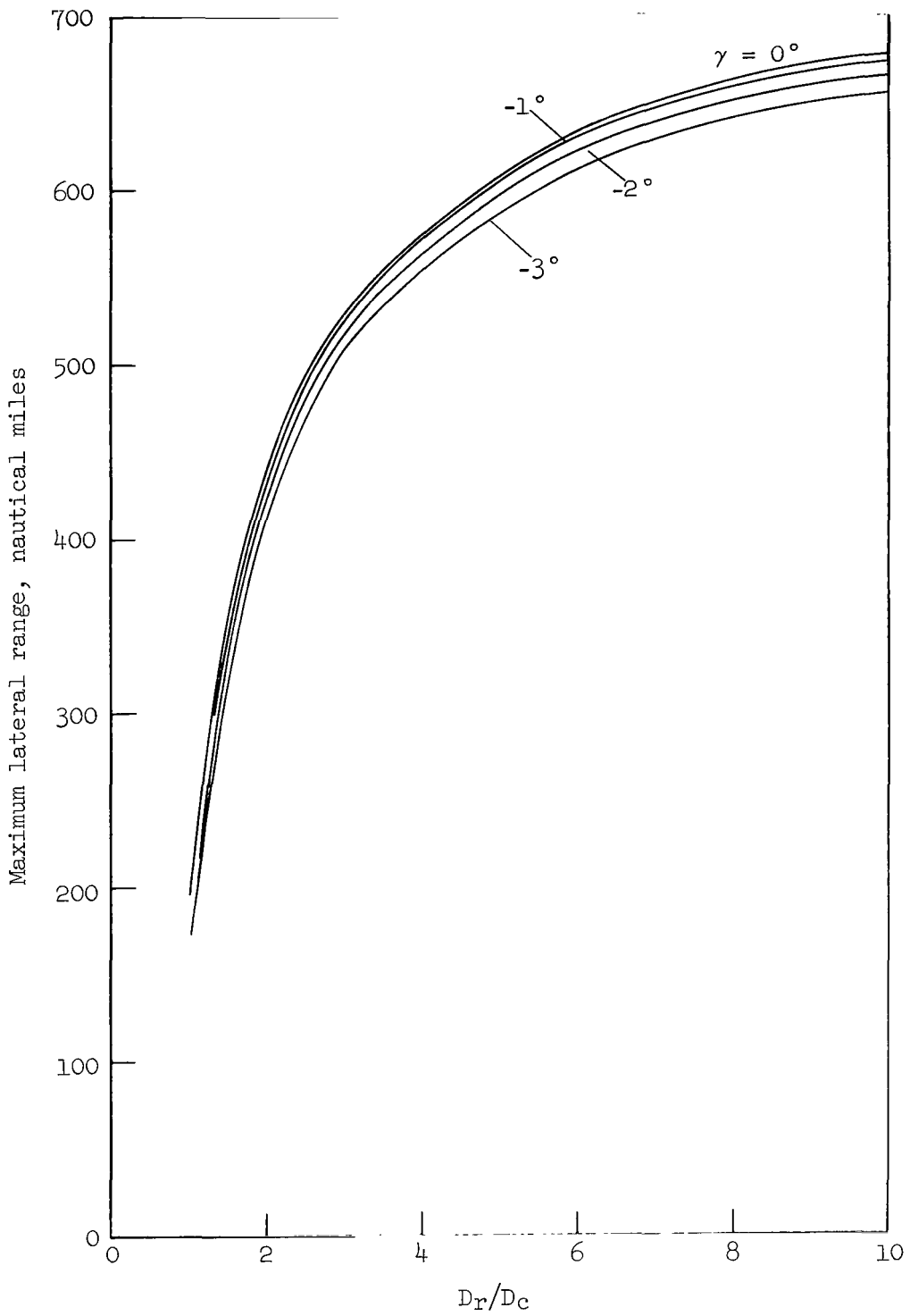
Figure 9.- Effect of diameter ratio on lateral range.
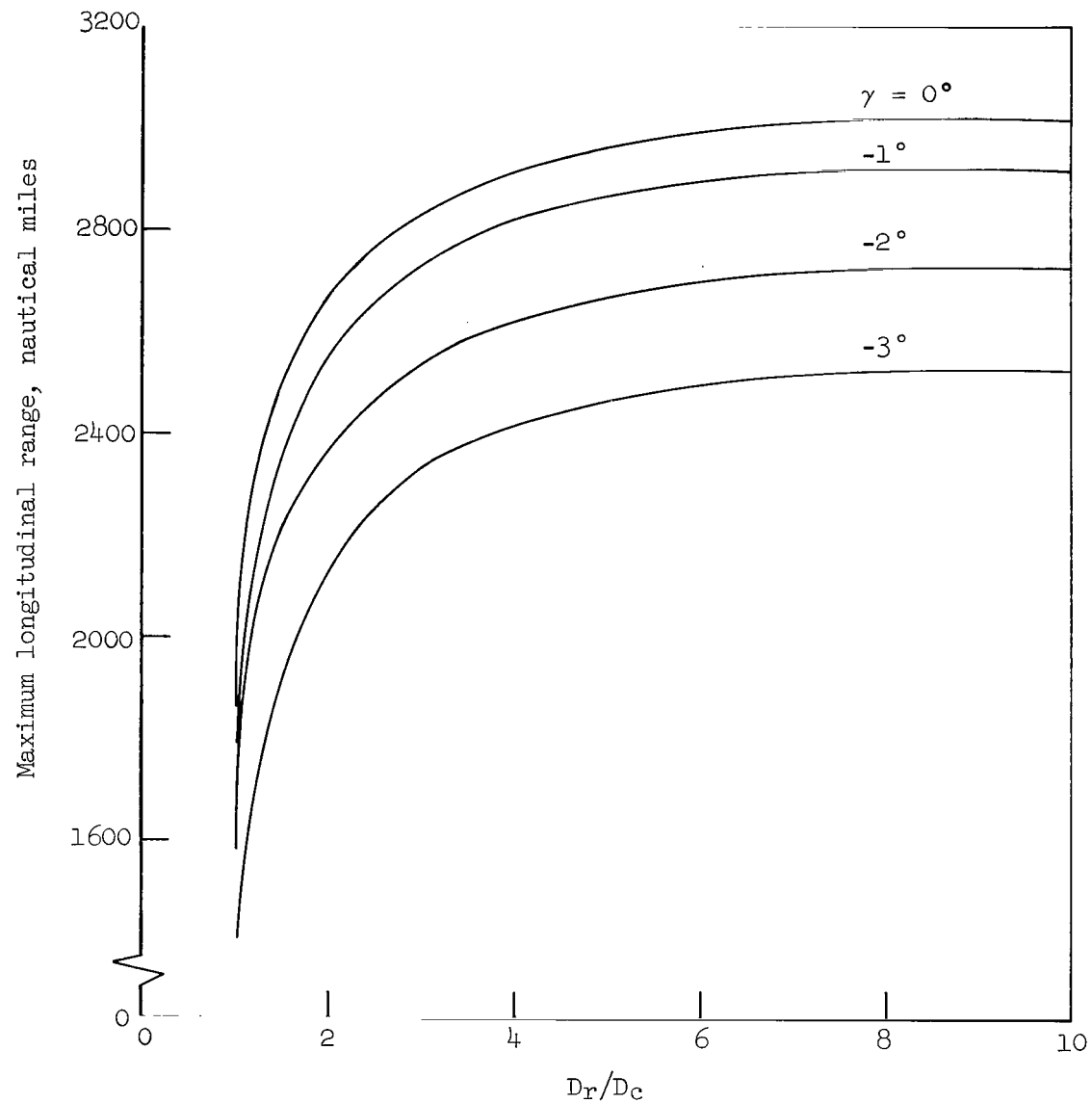
Figure 10.- Effect of diameter ratio on longitudinal range.
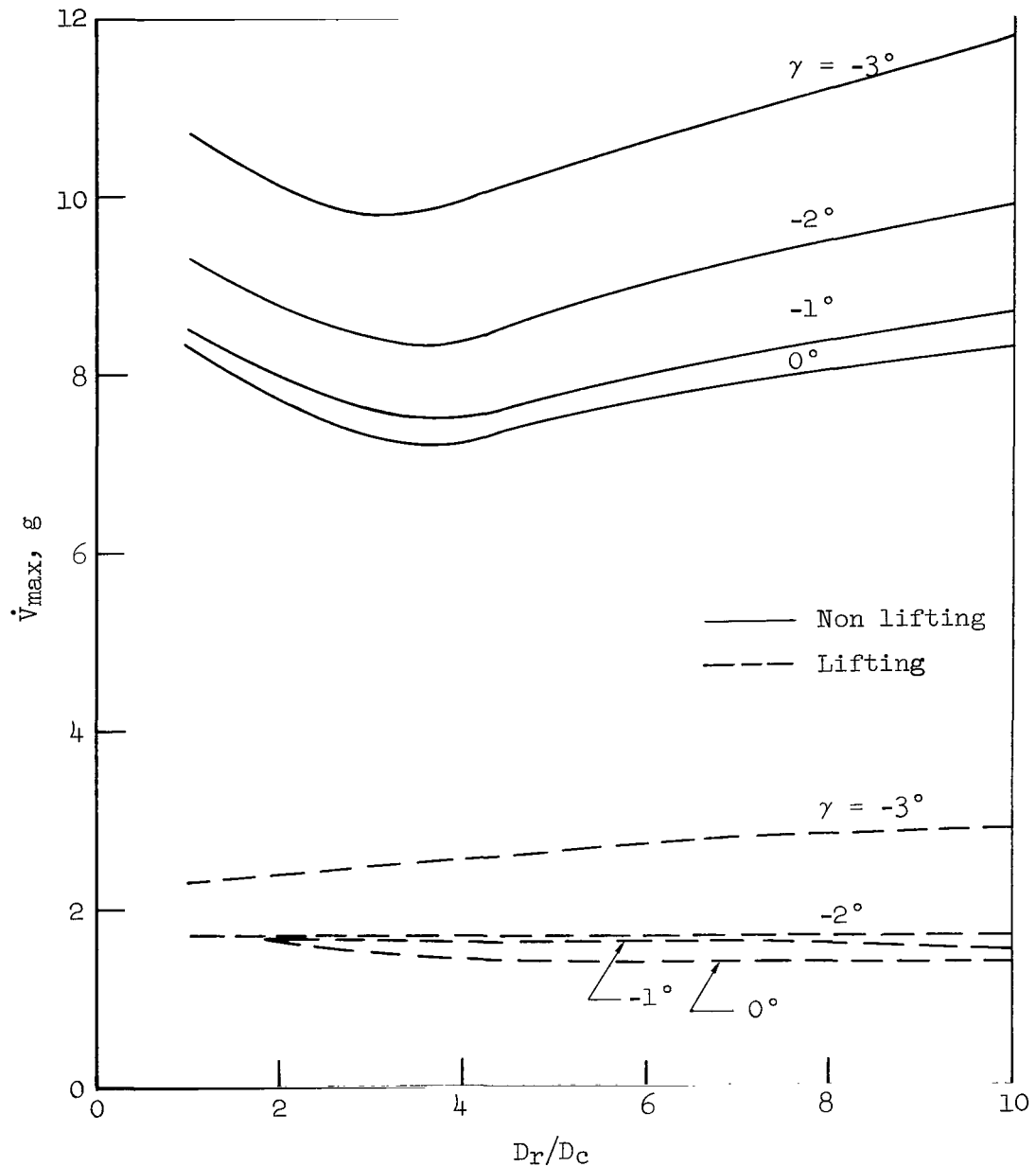
Figure 11.- Effect of diameter ratio on the decelerations.
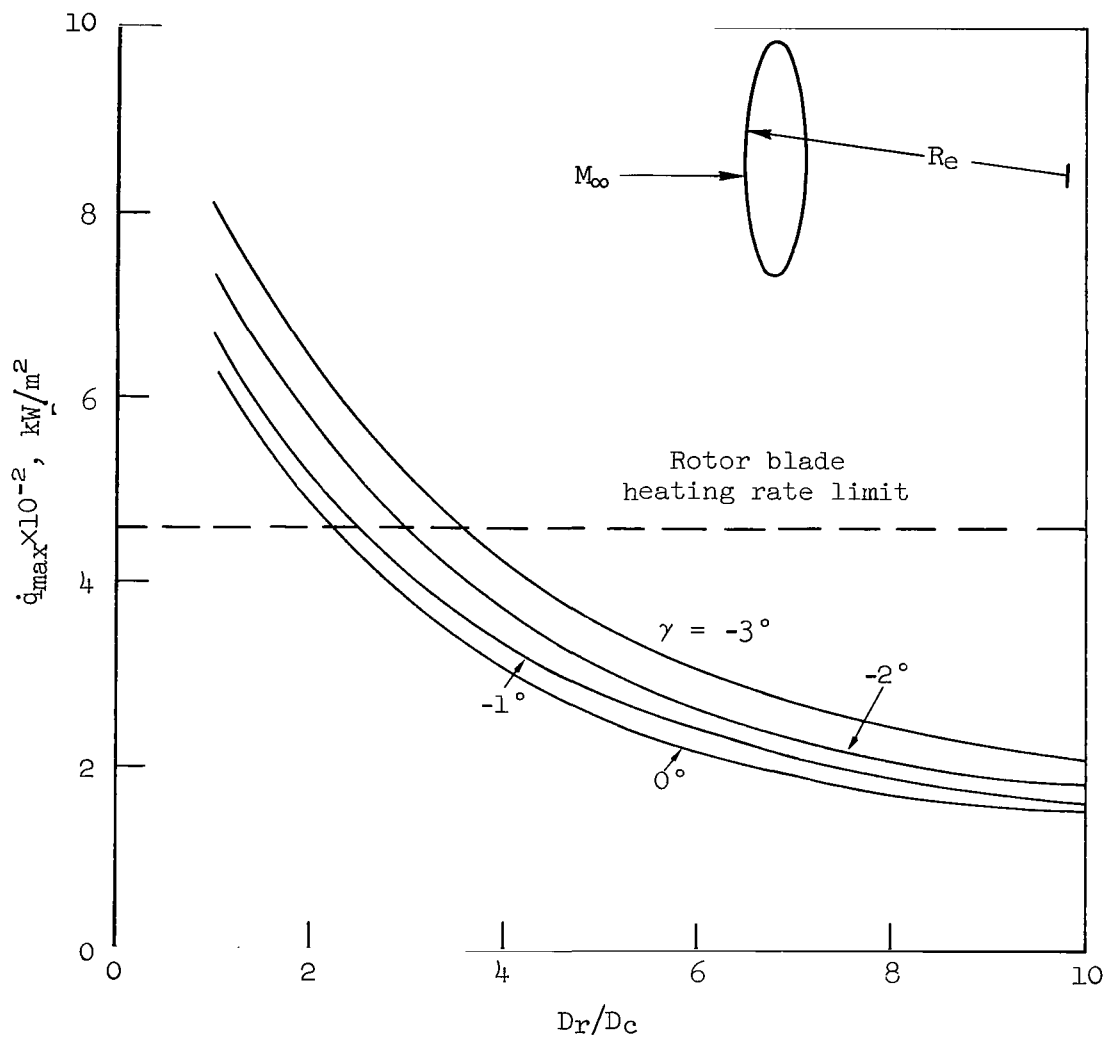
(a) Non lifting, $R_e = 1.524$ m (5 ft)

Figure 12.- Rotor blade maximum convective heating rate.
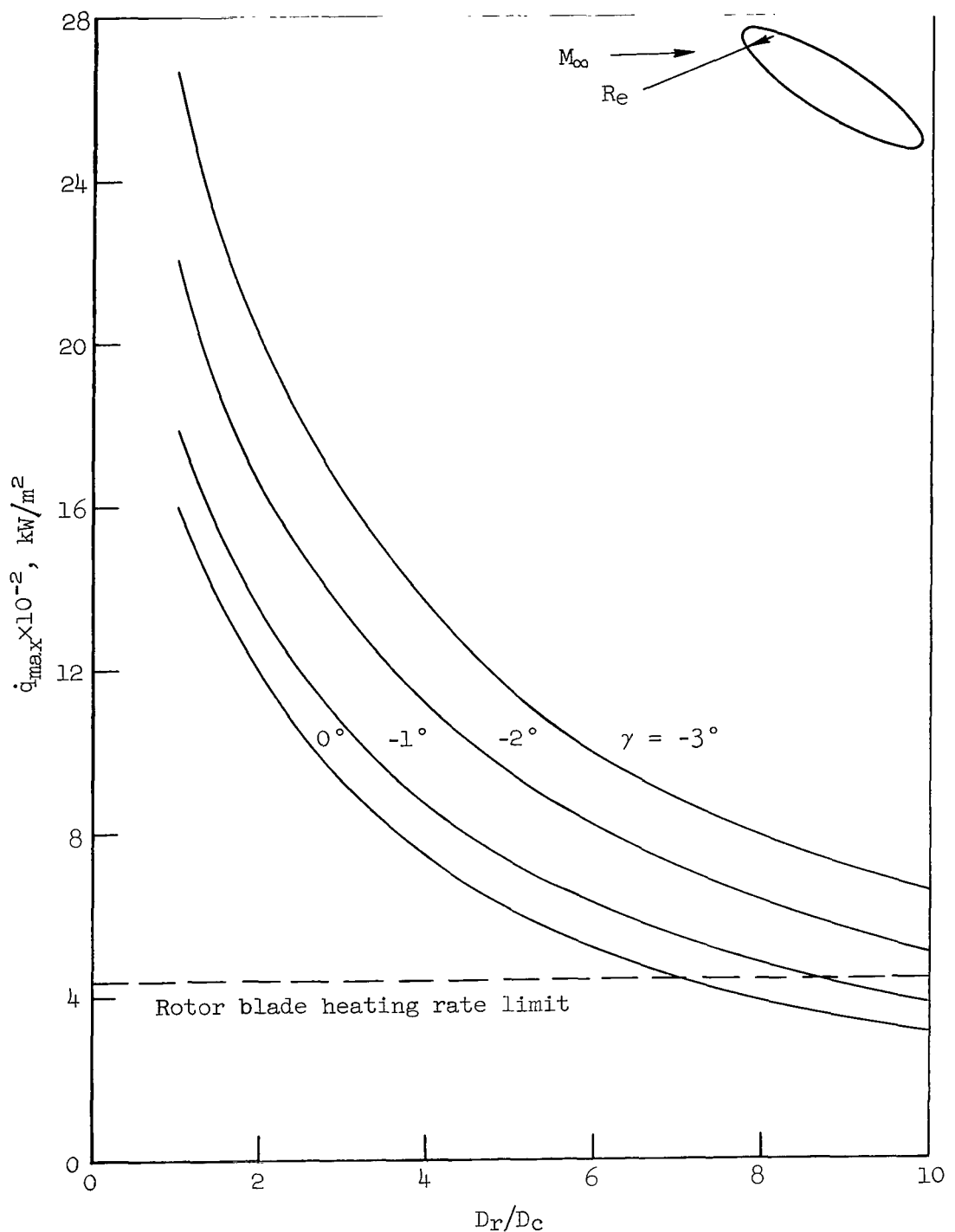
(b) Lifting, $R_e = 0.152$ m (0.5 ft)

Figure 12.- Concluded.
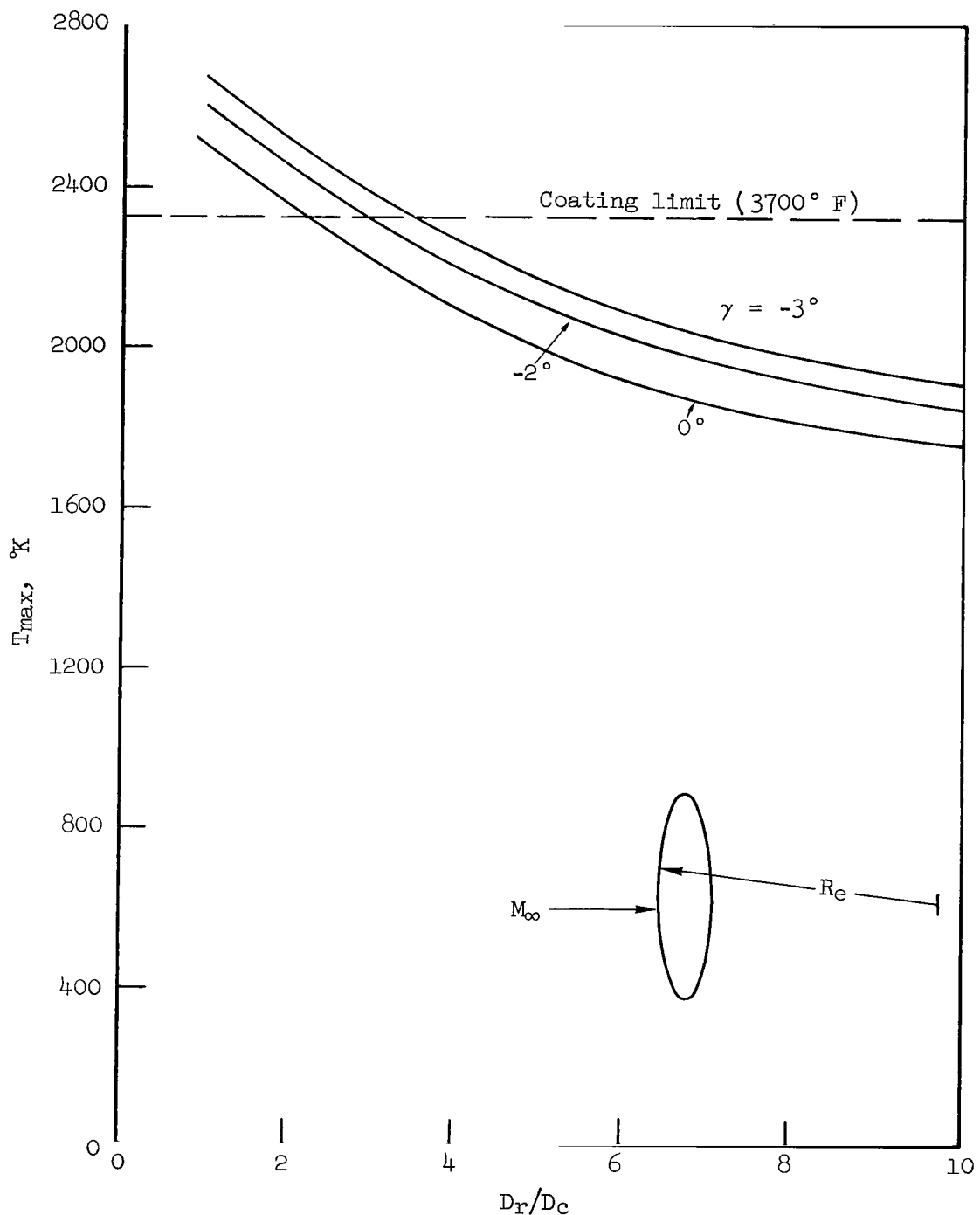
(a) Non lifting, R_e = 1.524 m (5 ft)

Figure 13.- Effect of diameter ratio on maximum blade temperature.
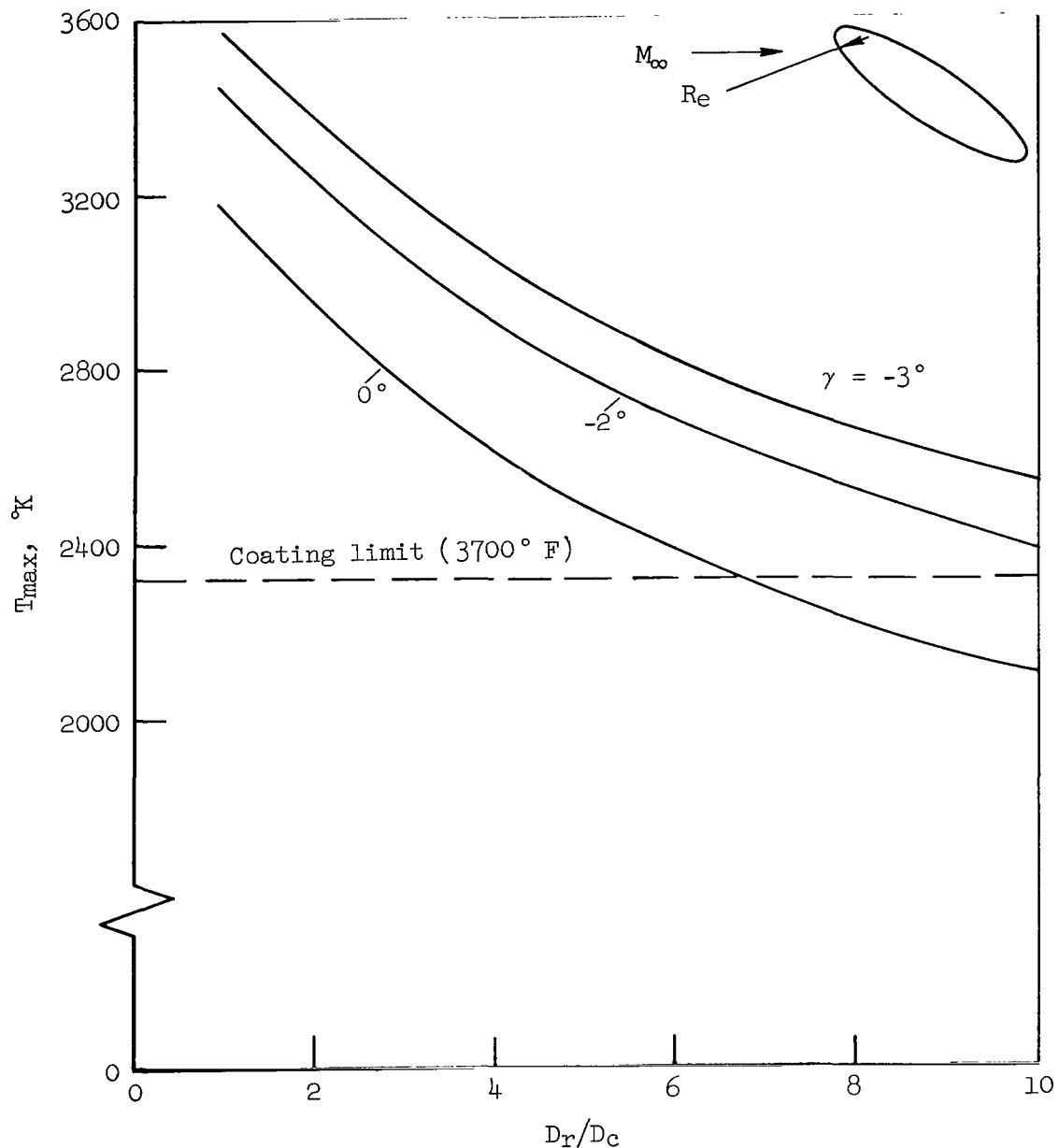
(b) Lifting, $R_e = 0.152$ m (0.5 ft)

Figure 13.- Concluded.
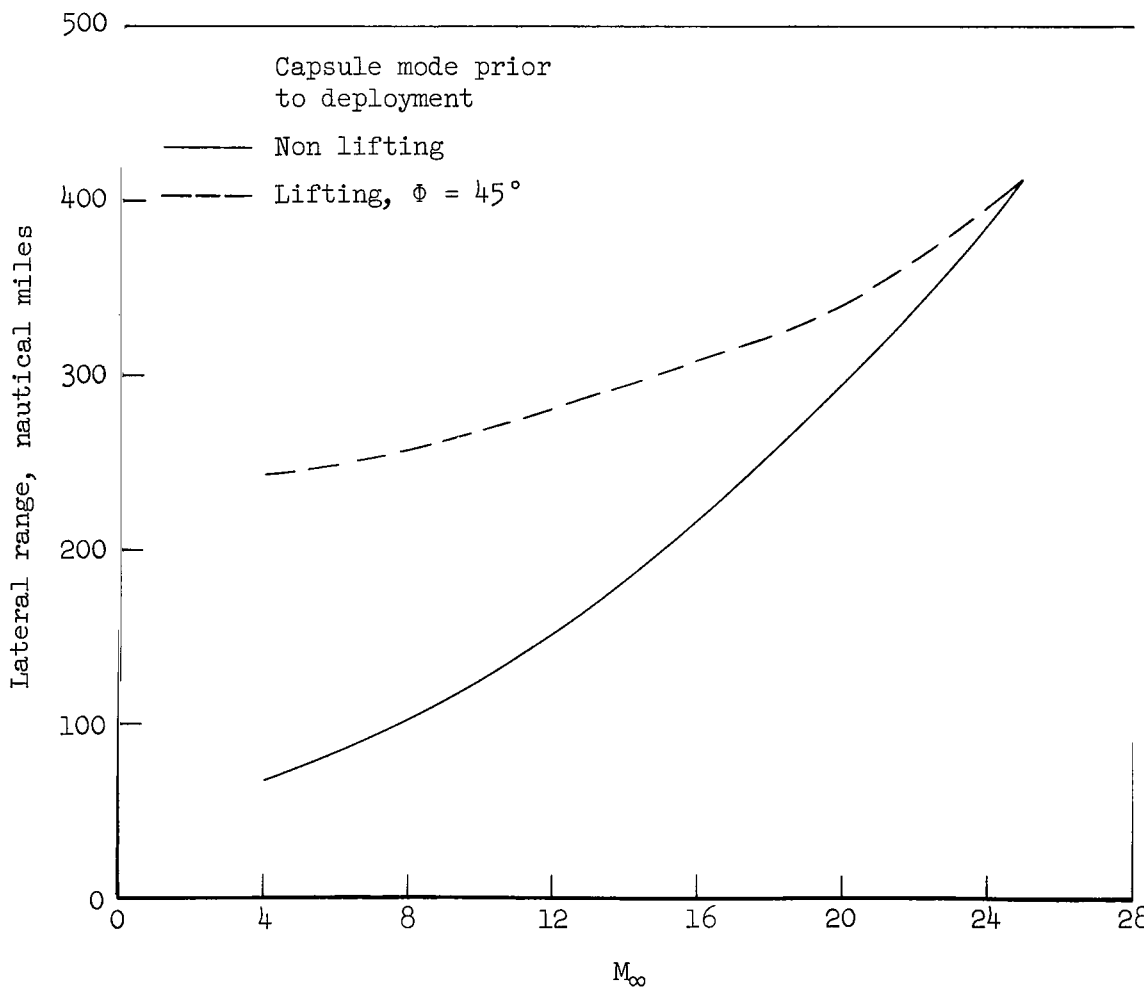
Figure 14.- Lateral range as a function of deployment Mach number; $\gamma = -3°$, $D_r/D_c = 2$.
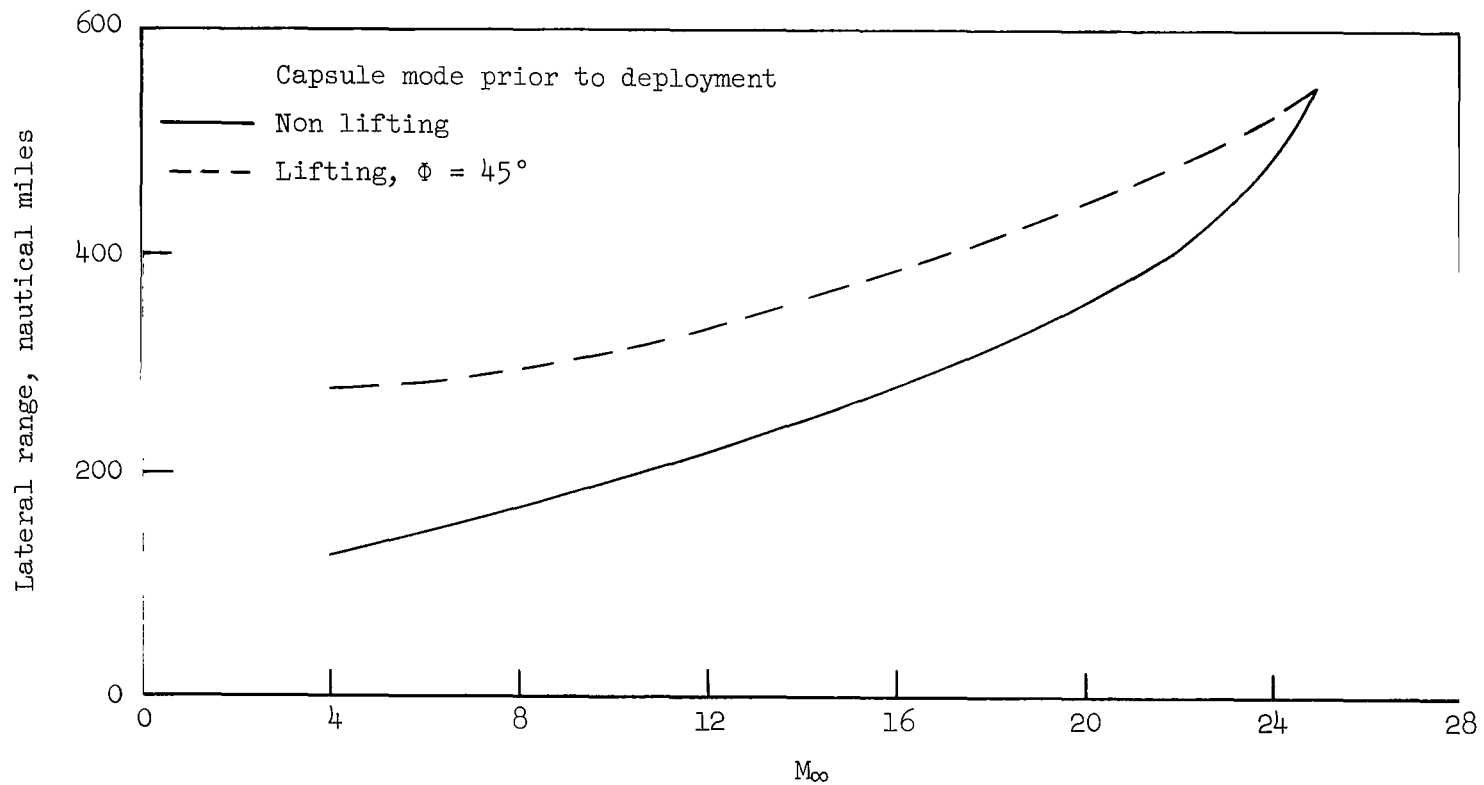
Figure 15.- Effect of deployment Mach number on lateral range; $\gamma = -3°$, $D_r/D_c = 4$.
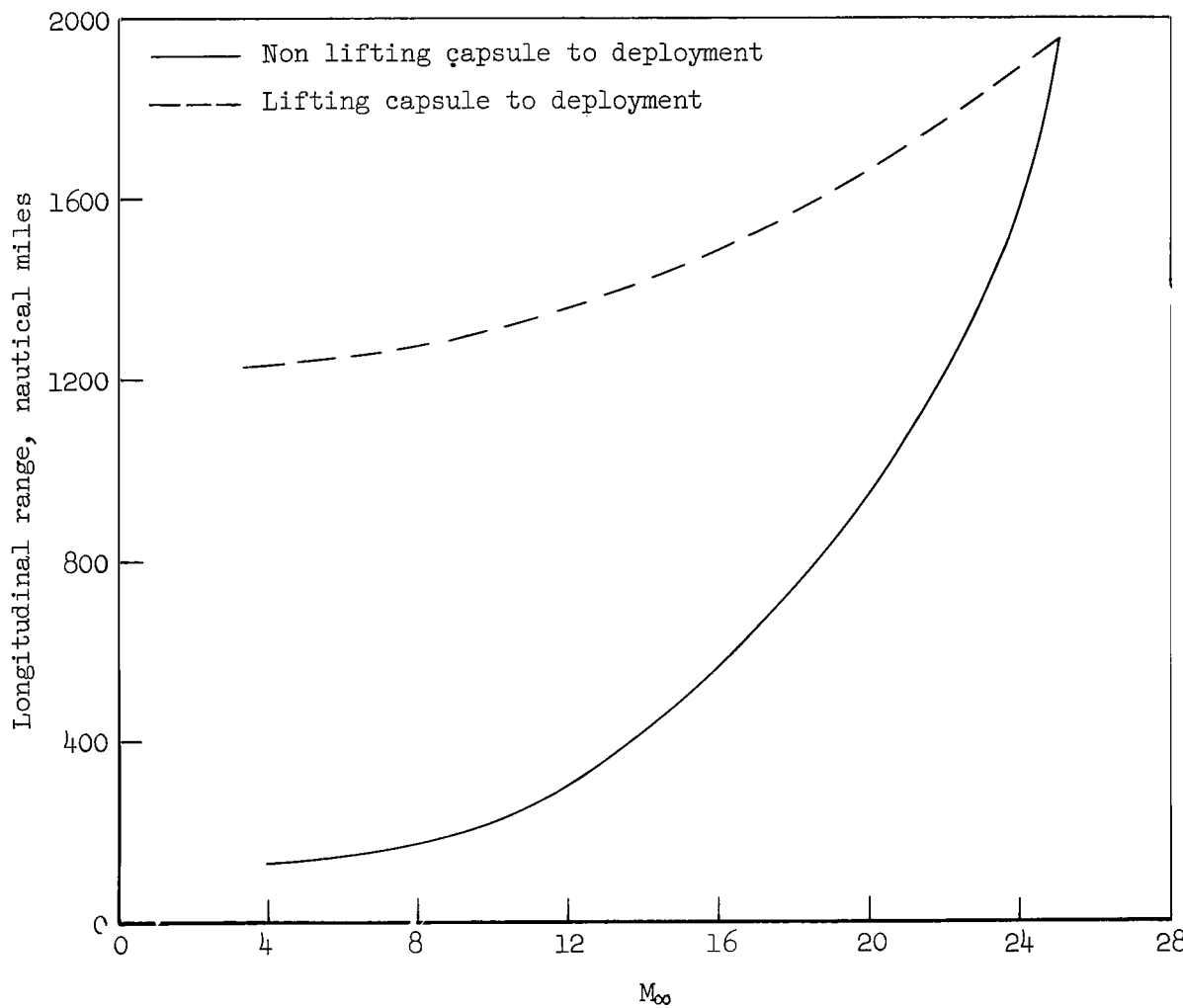
Figure 16.- Longitudinal range as a function of deployment Mach number; $\gamma = -3°$, $D_r/D_c = 2$.
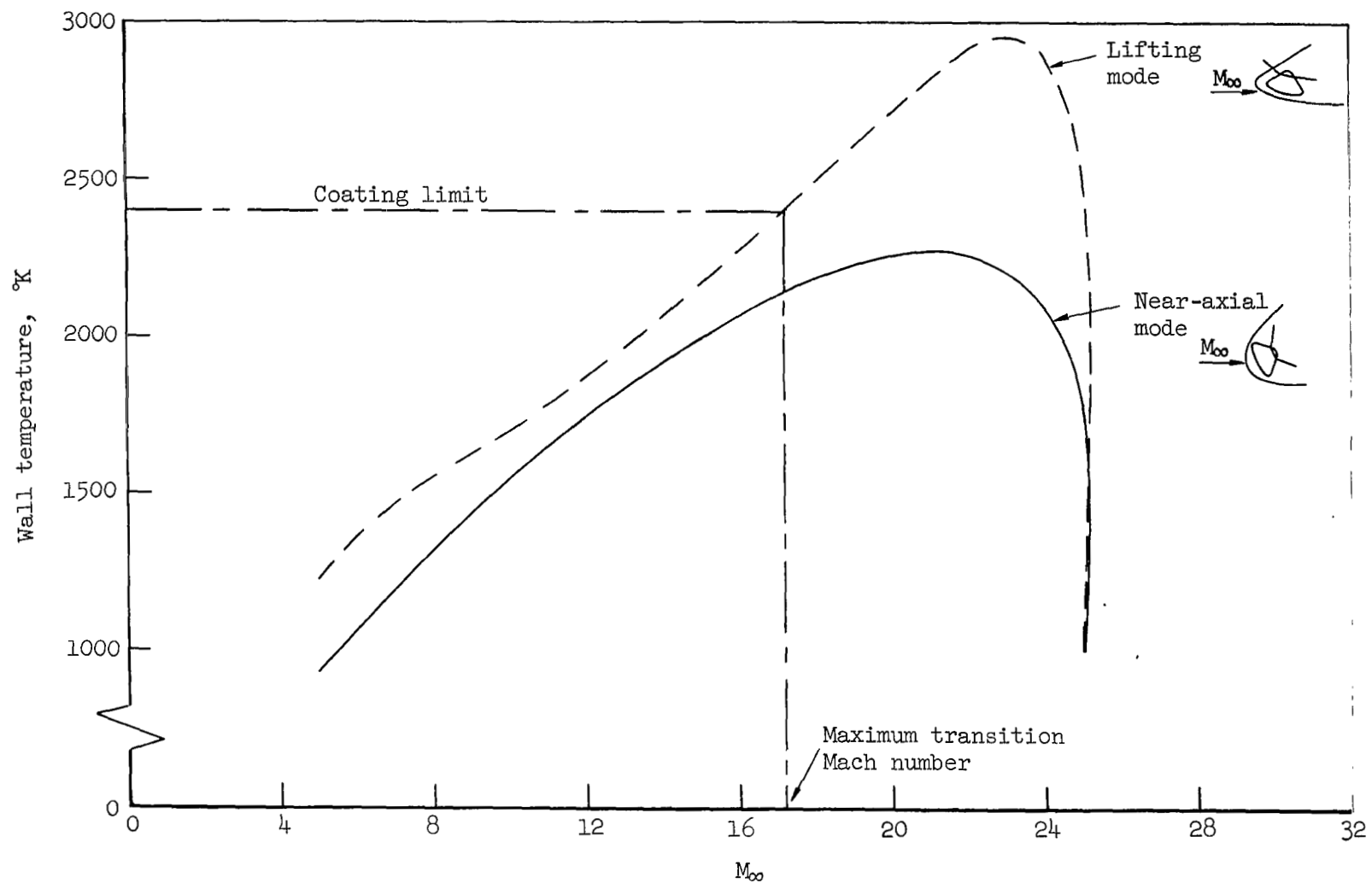
Figure 17.- Stagnation-point wall temperature; $\gamma = -2°$, $D_r/D_c = 4$.
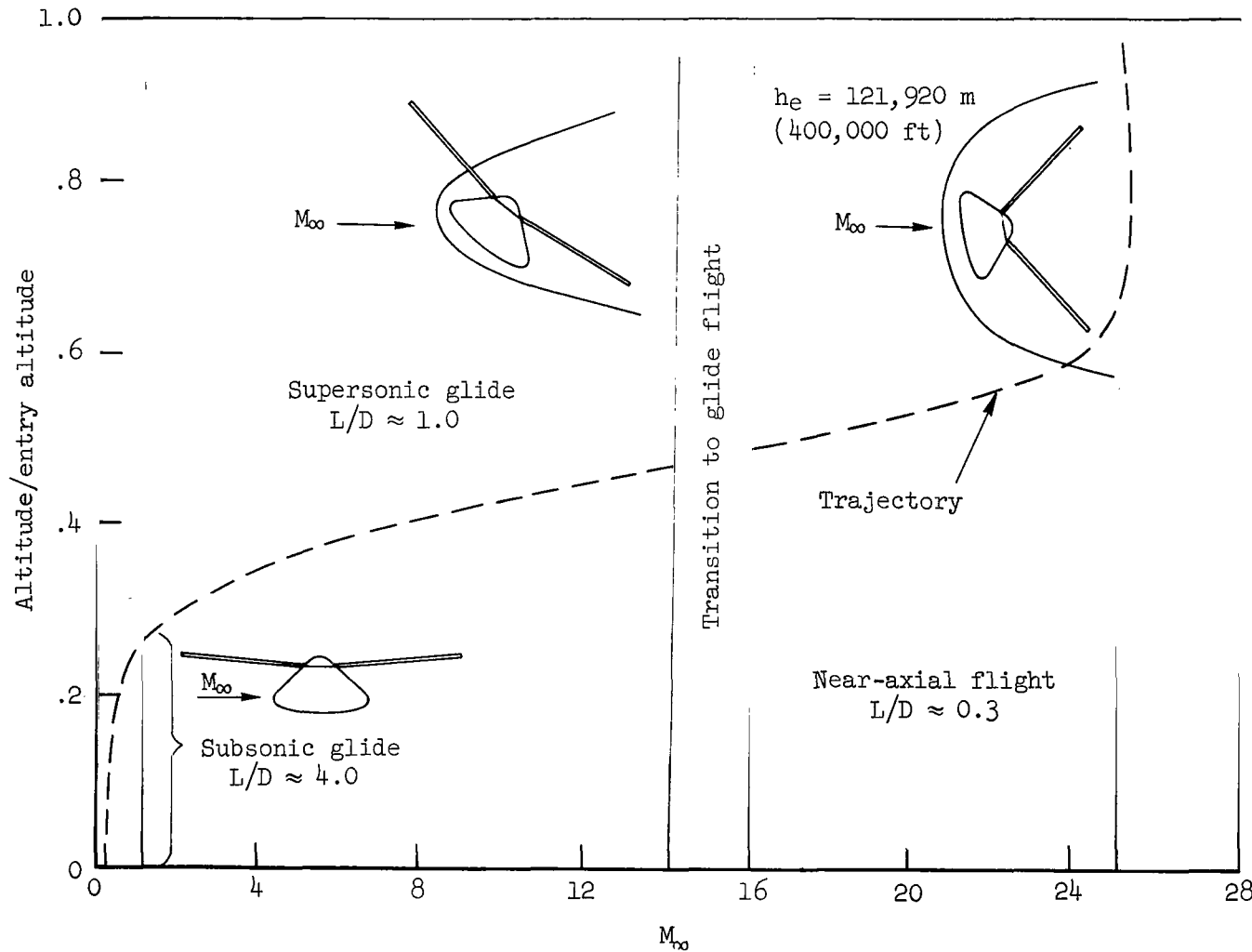
Figure 18.- Rotor vehicle operating modes.

FIRST CLASS MAIL

17U 001 56 51 3DS 68106 03903
AIR FORCE WEAPONS LABORATORY/AFWL/
KIRTLAND AIR FORCE BASE, NEW MEXICO 8711.

"The aeronautical and space activities of the United States shall be conducted so as to contribute . . . to the expansion of human knowledge of phenomena in the atmosphere and space. The Administration shall provide for the widest practicable and appropriate dissemination of information concerning its activities and the results thereof."

—NATIONAL AERONAUTICS AND SPACE ACT OF 1958

NASA SCIENTIFIC AND TECHNICAL PUBLICATIONS

TECHNICAL REPORTS: Scientific and technical information considered important, complete, and a lasting contribution to existing knowledge.

TECHNICAL NOTES: Information less broad in scope but nevertheless of importance as a contribution to existing knowledge.

TECHNICAL MEMORANDUMS: Information receiving limited distribution because of preliminary data, security classification, or other reasons.

CONTRACTOR REPORTS: Scientific and technical information generated under a NASA contract or grant and considered an important contribution to existing knowledge.

TECHNICAL TRANSLATIONS: Information published in a foreign language considered to merit NASA distribution in English.

SPECIAL PUBLICATIONS: Information derived from or of value to NASA activities. Publications include conference proceedings, monographs, data compilations, handbooks, sourcebooks, and special bibliographies.

TECHNOLOGY UTILIZATION PUBLICATIONS: Information on technology used by NASA that may be of particular interest in commercial and other non-aerospace applications. Publications include Tech Briefs, Technology Utilization Reports and Notes, and Technology Surveys.

Details on the availability of these publications may be obtained from:

SCIENTIFIC AND TECHNICAL INFORMATION DIVISION

NATIONAL AERONAUTICS AND SPACE ADMINISTRATION

Washington, D.C. 20546